

Study of Lithium Rich Giants with the GALAH Spectroscopic Survey

Deepak¹★ and Bacham E. Reddy¹

¹*Indian Institute of Astrophysics, Bangalore 560034, India*

Accepted January 10, 2019. Received January 10, 2019; in original form December 12, 2018

ABSTRACT

In this article, we speculate on the possible mechanisms for Li enhancement origin in RGB stars based on a large data set of around 340,299 stars collected from the GALAH survey combined with the Gaia astrometry. Data has 51,982 low mass ($M \leq 2M_{\odot}$) RGB stars with reliable atmospheric parameters. The data set shows a well populated RGB with well-defined luminosity bump and red clump with significant number of stars at each of these two key phases. We found 335 new Li-rich RGB stars with Li abundance, $A(\text{Li}) \geq 1.80 \pm 0.14$ dex, of which 20 are super Li-rich with $A(\text{Li}) \geq 3.20$ dex. Most of them appear to be in the red clump region which, when combined with stellar evolutionary timescales on RGB, indicates that the Li enhancement origin may lie at RGB tip during He-flash rather than by external source of merging of sub-stellar objects or during luminosity bump evolution. Kinematic properties of sample stars suggest that Li-rich giants are relatively more prevalent among giants of thin disk compared to thick disk and halo.

Key words: Surveys – Hertzsprung–Russell and colour-magnitude diagrams – Stars: evolution – Stars: abundances – Nucleosynthesis – stars: Li rich giants

1 INTRODUCTION

Measured abundance of $A(\text{Li}) = 3.32$ dex in young stars and interstellar medium (ISM) suggest that Li enriched significantly in the Galaxy from primordial value of $A(\text{Li}) = 2.72$ dex, a value predicted from the big bang nucleosynthesis (BBN) models based on the results from WMAP (Cerburt et al. 2008). One of the known sources for Li enrichment, apart from cosmic ray spallation (Mitler 1972), an interaction of high energy cosmic ray particles with carbon and oxygen atoms, and novae explosions (Tajitsu et al. 2015; Izzo et al. 2015), is nucleosynthesis in evolved stars. Though, stars, in general, are considered as Li sinks, highly evolved stars such as asymptotic giant branch (AGB) stars are known to produce fresh Li (Smith & Lambert 1989) via Cameron-Fowler mechanism (Cameron & Fowler 1971) which add to the Li enrichment of the Galaxy through mass loss. It is understood Li production in AGB happens only in relatively massive stars of $M \geq 3 M_{\odot}$ through a process known as hot bottom burning (Mowlavi 1995; Lattanzio et al. 1996). However, the discovery of high Li abundance in relatively less evolved low mass red giant branch (RGB) stars was unexpected (Wallerstein & Sneden 1982). Since then, observational studies revealed more Li-rich giants, and systematic surveys suggest Li-rich giants are rare, $< 1\%$ (e.g.,

Brown et al. 1989; Charbonnel & Balachandran 2000; Kumar et al. 2011). There are close to 200 Li-rich RGB stars (Casey et al. 2016) known so far with $\text{Li} \geq 1.5$ dex, an upper limit commonly used in the literature and attributed to the standard models of 1st-dredge-up on RGB (Iben 1967). In some cases, Li abundance was found to be more than the star’s initial abundance of $A(\text{Li}) = 3.2$ dex, which are known as super Li-rich giants (e.g., Kumar et al. 2011; Yan et al. 2018). In fact, observations in general, show much less Li than the expected limit (Fields 2011) and are attributed to extra-mixing process, post 1st dredge-up, during luminosity bump evolution (Deliyannis 1990), which is not part of the standard models. Thus, Li enhancement in RGB giants is a puzzle and its origin is being debated since a few decades.

There are two main hypotheses proposed for high Li in RGB stars: addition of Li rich material through merger of sub-stellar objects or internal nucleosynthesis and mixing-up of fresh Li with photosphere. There is no consensus on any of these two hypotheses. If the mechanism is in-situ nucleosynthesis as suggested by a few studies (Cameron & Fowler 1971; Mowlavi 1995; Lattanzio et al. 1996), RGB stars should be counted for Li enrichment in the Galaxy. On the other hand, if the enhancement is due to an external origin, we are simply observing the locked-up Li in sub-stellar objects. Thus, understanding the mechanism of Li enhancement in RGB may not only provide clues to our

★ E-mail: Deepak@iiap.res.in

2 Deepak and Reddy, B. E.

understanding of RGB nucleosynthesis, but to the larger issue of Li enrichment in the Galaxy.

The clue probably lies in finding the evolutionary phase of Li-rich giants on RGB. Evolutionary phase may be determined either by using star's position in the HR diagram or using asteroseismology (Bedding et al. 2011; Vrard et al. 2016) or secondary calibrations based on asteroseismology (Ting et al. 2018). Most of the currently known Li-rich giants have been classified based on their positions in the HR diagram. Due to small separation in values of luminosity and T_{eff} between different phases on RGB, in particular between the red clump and the luminosity bump, there are conflicting reports in the literature about the true evolutionary phase of Li-rich giants on RGB. With regards to asteroseismic analysis which has been proved to be a gold standard to separate He-core burning giants (red clump) from those of H-core burning giants ascending RGB for the first time. Asteroseismic data is mostly based on either Kepler or CoRoT missions. Unfortunately data is not available for all the stars as these observations are made for specific sky fields. Presently, evolutionary phase is accurately known, based on Kepler asteroseismic data and CoRoT asteroseismic data, only for half a dozen Li-rich stars (Silva Aguirre et al. 2014; Jofré et al. 2015; Bharat Kumar et al. 2018; Singh et al. 2019; Smiljanic et al. 2018). Interestingly, all of them are red clump stars with He-core burning except the star studied by Jofré et al. (2015) which is on RGB with H-core burning phase whose Li-rich giant status is discussed later in the discussion section. None of the previously known Li-rich giants are in the Kepler field.

This necessitates to explore alternate ways to find the evolutionary phase of Li-rich giants. One of the ways is to undertake large scale survey for Li-rich giants in globular clusters which have well defined RGB with visible luminosity bump and red clump with significant number of stars. However, getting a reasonable resolution spectra for a large number of fainter stars in globular clusters even with 10-m class telescopes is difficult and time consuming. Another way is to employ a large data set of giants with measured Li abundance and accurate astrometry.

Fortunately, while analyzing large data sets from the Gaia and the GALAH spectroscopic surveys to understand elemental abundance patterns in the Galaxy, we noticed a strikingly well populated red clump and RGB in the HR diagram of $L-T_{\text{eff}}$ of the GALAH stars. This could, potentially, be used to find clues to Li enhancement origin in RGB stars if we search for Li enhanced giants along the RGB. Combining the Gaia astrometry and the GALAH Li abundances, we provide an evidence that most of the Li-rich stars belong to the red clump with implications for Li enhancement origin scenarios.

2 STELLAR SAMPLE

The Galactic Archeology with HERMES (GALAH) spectrograph is a large scale spectroscopic survey of spectral resolution of $R (= \Delta\lambda/\lambda) \approx 28,000$ with spectrograph attached to 4-m Anglo-Australian Telescope (AAT). In the GALAH DR2 (GALAH Data Release 2), the GALAH team has provided quantitatively derived abundances of about 23 elements including the light element Li, which is the focus

of this article, for a sample of 342,682 stars (see Buder et al. 2018). The sample is searched for corresponding astrometric and photometric data from the Gaia Data Release 2 (hereafter the Gaia DR2) of 1.7 billion stars. Source matching is done using the Gaia DR2 source identifier provided in the GALAH DR2 data set (see Buder et al. 2018; Gaia Collaboration et al. 2018). This resulted in a sample of 340,299 common stars among the two data sets. Further, we culled out stars for which $\sigma_{\text{Teff}_{\text{GALAH}}} \geq 100$ k, parallax (π) is negative and fractional error in parallax, $\sigma_{\pi}/\pi \geq 0.15$ yielding a total sample of 246,390 stars.

The GALAH also provides an index of $\text{Flag}_{\text{Cannon}}$ against each star which indicates accuracy or level of confidence in derived stellar parameters. $\text{Flag}_{\text{Cannon}}$ index range from 0 to 128, with 0 being the most reliable, and other numbers indicating issues such as binary companion, fitting accuracies, S/N ratio, etc. (for more details see Buder et al. 2018). We restricted our sample to stars with reliable stellar parameters by culling out all the stars with nonzero value of $\text{Flag}_{\text{cannon}}$. This yielded a total of 204,370 stars.

In addition, to avoid stars of higher masses of early AGB and stars evolved from hotter spectral types from main sequence, as some of them are found to be having higher Li abundances due to inefficient mixing, we have restricted our sample to low mass RGB stars of $M \leq 2M_{\odot}$, which are expected to evolve through both luminosity bump and He-flash (Carlberg et al. 2016; Cassisi et al. 2016). Masses have been estimated using the formula, $M/M_{\odot} = 10^{[\log(L/L_{\odot}) + \log(g) - 4 \times \log(T_{\text{eff}}_{\odot}/T_{\text{eff}})]}$, where we used $\log(g) = 4.44$ dex and $T_{\text{eff}} = 5772$ K for solar values. Values of effective temperature, $T_{\text{eff}_{\text{GALAH}}}$, and logarithmic surface gravity, $\log(g)$, are adopted from the GALAH catalog (Buder et al. 2018) and the values of luminosities are based on parallaxes and apparent magnitudes taken from the Gaia catalogue. We used bolometric correction based on $T_{\text{eff}_{\text{GALAH}}}$ and relation given in Andrae et al. (2018). Values of luminosities given in the Gaia and those derived in this study using $T_{\text{eff}_{\text{GALAH}}}$ agrees well with each other. The difference between the two values is quite small with $\sigma \approx 0.02$ dex. Uncertainties in the derived luminosity values due to errors in parallax and $T_{\text{eff}_{\text{GALAH}}}$ are also estimated and are found to be quite small, typically $\sigma_{L/L_{\odot}} \leq 0.05$ dex for most of the stars. With this, we have a final sample of 188,679 low mass stars.

3 ANALYSIS

3.1 Sample stars in $L - T_{\text{eff}}$ plane

Sample data plotted in the HR-diagram of Luminosity versus effective temperature (Figure-1) shows stellar evolution with well defined main sequence and red giant branch. Since our interest lies in the Li enhancement during RGB evolution, RGB has been separated from the data set as defined by a box with dash-line in Figure-1. The box includes giants from the base of RGB through its tip and red clump in the $L - T_{\text{eff}}$ plane defined by $3800\text{K} \leq \text{Teff}_{\text{GALAH}} \leq 5200\text{K}$ and $0.3 \leq \log(L/L_{\odot}) \leq 3.0$. This yielded 51,982 red giant branch stars which are the focus of this study. The data sets also show two visible concentrations of stars which are identified as luminosity bump and red clump regions and have been marked by red and black rectangles, respectively. The

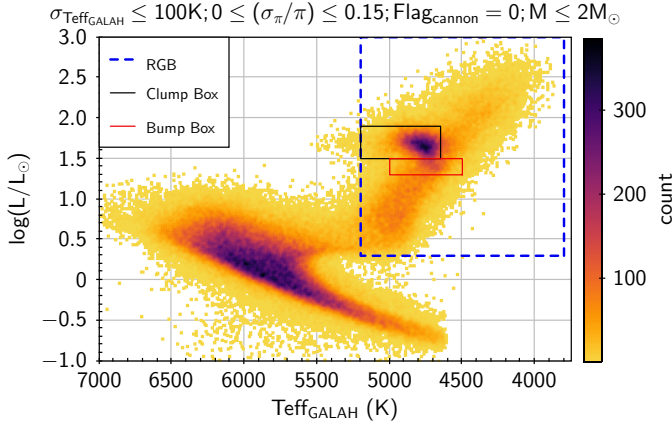


Figure 1. Sample stars in the HR diagram.

two clusters are defined in L - T_{eff} plane by (1.5, 1.9; 4650, 5200) for red clump and (1.3, 1.5; 4500, 5000) for the luminosity bump. The concentrations at these two phases are direct consequences of their relatively longer evolutionary timescales compared to any other place on RGB. The well defined stellar concentrations could be used to decipher the origin of Li excess by searching for Li-rich giants among the well defined RGB, luminosity bump and red clump.

3.2 Li abundances of sample stars

The GALAH DR2 provides Li abundances in the form of $[\text{Li}/\text{Fe}] (= [\text{Li}/\text{H}] - [\text{Fe}/\text{H}])$, where $[\text{Li}/\text{H}] = A(\text{Li}) - A(\text{Li})_{\odot}$ along with associated error and a flag indicating the level of confidence in the measured abundance. The GALAH also provides metallicity, $[\text{Fe}/\text{H}]$, for all the stars in the catalogue. Commonly, Li abundance is expressed as $A(\text{Li}) = \log(n(\text{Li})/n(\text{H})) + 12$. For a better comparison with the literature, $[\text{Li}/\text{Fe}]$ values of the GALAH are converted into $A(\text{Li})$ using the expression $A(\text{Li}) = [\text{Li}/\text{Fe}] + [\text{Fe}/\text{H}] + A(\text{Li})_{\odot}$, where $A(\text{Li})_{\odot}$ is the solar Li abundance. We adopted $A(\text{Li})_{\odot} = 1.05 \pm 0.10$ dex, which is the same one used for the GALAH data (see Buder et al. 2018). The corresponding error is $\sigma_{A(\text{Li})} = (\sigma_{[\text{Li}/\text{Fe}]}^2 + \sigma_{[\text{Fe}/\text{H}]}^2 + 0.10^2)^{1/2}$.

Level of confidence in measured lithium abundances of the sample has been encoded in the form of lithium abundance flag, $\text{Flag}_{[\text{Li}/\text{Fe}]}$, against each star. $\text{Flag}_{\text{Abundance}}$ index ranges from 0 to 9, with 0 being the most reliable, flag one is raised when line strength is below 2σ , flag two is raised when cannon fitting started extrapolating, flag three is when both flag one and two are raised, flag four is when χ^2 of best fitting model spectrum is very high or low, flag eight is raised when $\text{Flag}_{\text{cannon}}$ is not zero, and the remaining flags are combinations of these flags (see Buder et al. 2018, for more details). On checking, we found that all the stars with relatively higher value of Li, for example $A(\text{Li}) \geq 1.6$ dex, has $\text{Flag}_{[\text{Li}/\text{Fe}]} \leq 3$, while for some of the Li-low stars $\text{Flag}_{[\text{Li}/\text{Fe}]} \geq 3$. Higher $\text{Flag}_{[\text{Li}/\text{Fe}]}$ value for Li-low stars is expected as Li absorption line in those stars is weaker. We consider all RGB stars for which Li abundance is measured by the GALAH as this would enable us to comment on the relative fraction of Li-rich giants among RGB stars and evolution of Li itself along the RGB.

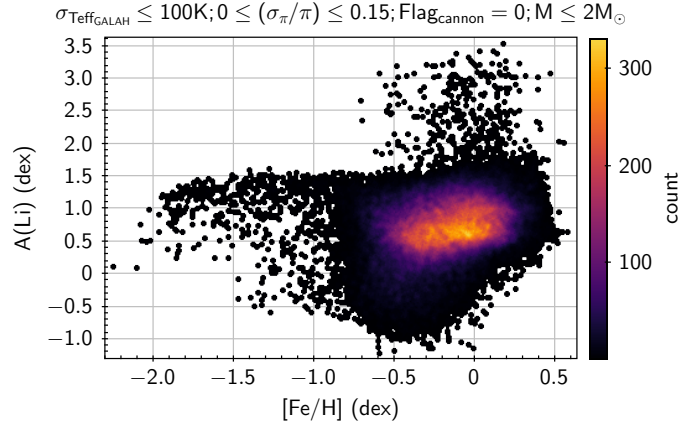


Figure 2. Lithium abundance versus metallicity of RGB sample stars.

4 RESULTS

4.1 Li-rich giants on RGB

Standard models of stellar evolution (Iben 1967) predict dilution of Li in RGB stars by a factor of 30 to 60 from its main sequence value. Models, however, do not prescribe the value of initial Li abundance on main sequence which is a function of age, mass, metallicity, and its pre-main sequence evolution (Lambert & Reddy 2004). If we assume RGB stars evolved off the main sequence with initial value of $A(\text{Li}) = 3.32$ dex, according to the standard models, one would expect $A(\text{Li}) \approx 1.5$ to 1.8 dex for RGB giants in the mass range of 1 to $1.5 M_{\odot}$, lower the mass, lesser is the dilution factor. However, in the literature, commonly a single upper limit of $A(\text{Li}) = 1.5$ dex is used for Li-normal giants, and giants with $A(\text{Li})$ higher than this are considered as Li-rich. But for the question “What is a Li-rich giant?”, answer seems to be not a single limit, but probably multiple limits depending on mass and metallicity. Also, see Smiljanic et al. (2016) and Aguilera-Gómez et al. (2016) who discussed lower limit for Li-rich giants in connection with two giants (Trumpler 20 MG 340 and 591) with $A(\text{Li}) \sim 1.6$ dex which is at the border line for qualifying them as Li-rich giants. Here, we use Li trends with metallicity to define Li abundance limits on RGB.

In a plot of $A(\text{Li})$ versus $[\text{Fe}/\text{H}]$ (Figure-2), one can notice varying Li trend with metallicity. The trend can be grouped into three: very metal-poor stars with $[\text{Fe}/\text{H}] \leq -1.5$ dex, metal poor stars with $-1.5 < [\text{Fe}/\text{H}] \leq -0.5$ dex, and metal-rich stars with $[\text{Fe}/\text{H}] > -0.5$ dex. The metal-poor giants show a well defined upper limit of $A(\text{Li}) \approx 1.5$ dex for Li-normal giants, which is commonly used in the literature. For very metal poor giants, the nice horizontal trend breaks down at $[\text{Fe}/\text{H}] = -1.5$ dex and Li abundance starts rapidly decreasing with decreasing $[\text{Fe}/\text{H}]$. Though it is interesting in the context of Li evolution in the early Galaxy, for the present study we concentrate on Li-rich giants among RGB. It is also interesting to note that there are no Li-rich giants among giants with $[\text{Fe}/\text{H}] \leq -0.7$ dex. However, on our loosely defined metal-rich side, the Li abundance upper limit for Li-normal stars seems to be slightly higher with a range

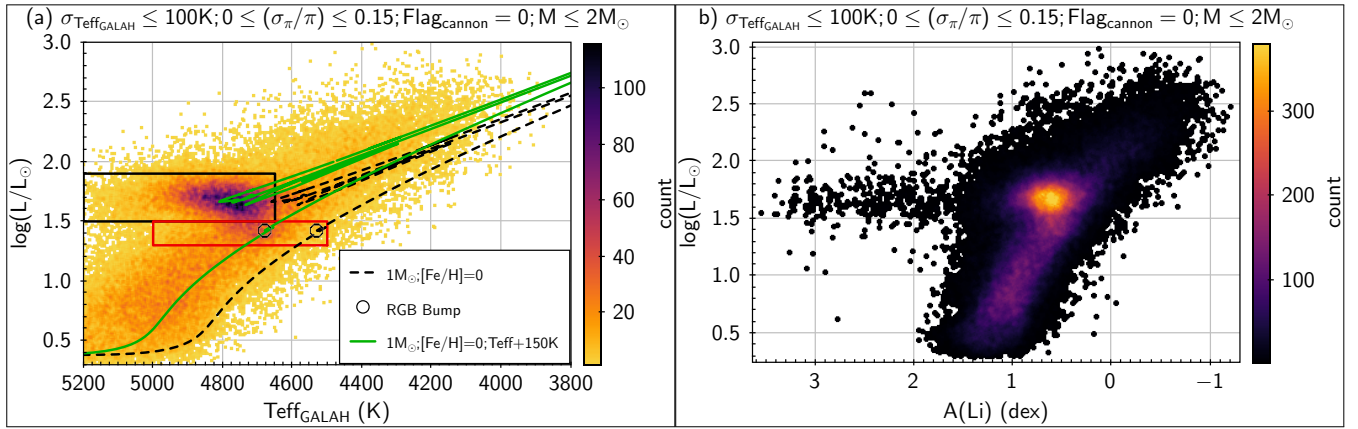


Figure 3. The HR diagram and $\log(L/L_{\odot})$ vs $A(\text{Li})$ distribution for our selected RGB sample stars from the GALAH DR2 and the Gaia DR2 survey with mass $M \leq 2M_{\odot}$. In Figure-3a, we have also shown the approximate positions of RGB bump (red rectangle) and RGB clump (black rectangle).

of $A(\text{Li}) \approx 1.6 - 1.8$ dex than the commonly used upper limit of $A(\text{Li}) = 1.5$ dex for Li-normal giants.

For the current study, we adopt a single limit of $A(\text{Li}) = 1.8$ dex, instead of using two upper limits, as most of the Li-rich giants in the sample are in the higher metallicity group (i.e. $[\text{Fe}/\text{H}] > -0.6$ dex) as shown in Figure-2. This is also the same upper limit set by standard models for low mass ($1M_{\odot}$) Li-normal giants. In addition, given the relatively larger uncertainties ($\approx \pm 0.14$) involved in the derivation of Li abundances from the spectra, adoption of a slightly higher limit to avoid contamination with Li-normal giants is justified. With this definition, we found 335 giants with $A(\text{Li}) \geq 1.8$ dex.¹ This is about 0.64% of total RGB giants considered in this study and confirms the previous survey results (Brown et al. 1989; Kumar et al. 2011; Kirby et al. 2012) that Li-rich giants are a rare group.

4.2 Stellar Evolutionary Phase of Li-rich Giants

Determination of stellar evolutionary phase of Li-rich giants is the key motivating factor of this study and has been elusive for a long time due to lack of large data set with Li abundances coupled with accurate astrometry. The current larger data set of the GALAH Li abundances and the Gaia astrometry is ideally suited for this purpose. In Figure-3, the selected sample of 51,982 giants for which Li abundances have been measured and have accurate T_{eff} and luminosity have been shown. Clump stars are concentrated within the luminosity range of $\log(L/L_{\odot}) = 1.5 - 1.9$ (blue rectangle). Bump stars appear to be slightly at a lower luminosity below the much larger group of clump stars. To demonstrate that RGB, bump and clump regions are well identified in the data (Figure-3), we superposed a representative theoretical evolutionary track of $1M_{\odot}$ star with $[\text{Fe}/\text{H}] = 0.0$, taken from MESA Isochrones & Stellar Tracks' latest version MISTv1.2 available at <http://waps.cfa.harvard.edu/>

¹ Stellar parameters of all the Li-rich giants in our sample will be provided as a supplementary table (online). Currently, data is given at the end of manuscript (see Table-3).

[MIST/index.html](#) and for details see Paxton et al. (2011). The solar like model is used as the mass and metallicity distribution of the current data set peaks at about $1M_{\odot}$ and $[\text{Fe}/\text{H}] = 0.0$ dex. However, the theoretical track is systematically cooler by about 150 K (Figure-3a, broken line). If the track is shifted by 150 K towards the hotter side, it coincides well with the observed locations of the bump and clump stars, and runs through the middle of RGB. Note, the theoretical models, due to differences in input assumptions, disagree by more than 100 K in T_{eff} among themselves and in some cases with observations (Salaris et al. 2002).

To test the occurrence of Li rich giants on RGB, we have shown in Figure-3b, a plot of Luminosity versus $A(\text{Li})$. It is known that Li abundance is a function of T_{eff} in which $A(\text{Li})$, in general, decreases with decreasing T_{eff} . As a result, the plot of $\log(L/L_{\odot})$ versus $A(\text{Li})$ (Figure-3b) mimics the HR diagram of $\log(L/L_{\odot})$ versus $T_{\text{eff,Galah}}$. Most of the giants follow this general rule and show, on an average, a decreasing Li trend as they ascend RGB towards the tip. Contrary to this general rule, however, a small group of giants show enhanced Li abundance, in particular, at a region which coincides with red clump, post He-flash. There are also Li-rich giants below and above the red clump luminosity range as indicated in Figure-3a. Interestingly, Li-rich giants with $\log(L/L_{\odot}) \leq 1.5$ are far less compared to those at the clump. Giants above the clump luminosity are probably early AGB stars about which we comment further in section 5.

It appears from Figure-3 that most of the Li-rich giants are concentrated at the red clump. Out of the total 335 Li-rich giants, as mentioned above, there are 253 that seem to fall in the red clump luminosity range of $L/L_{\odot} = 1.5 - 1.9$ dex (see Figure-3a). Bump with relatively lesser number of Li-rich giants (24), appears to be just below and rightwards of the clump, falls in the luminosity range of $L/L_{\odot} \approx 1.3 - 1.5$ dex. Given the small difference between the luminosities of red clump and RGB bump, about 0.3 dex (the difference between the mid values), and the typical errors in luminosities, about 0.05 dex (maximum 0.1 dex), we can not rule out the possibility of small overlap of giants among bump and clump. There are also a few Li-rich

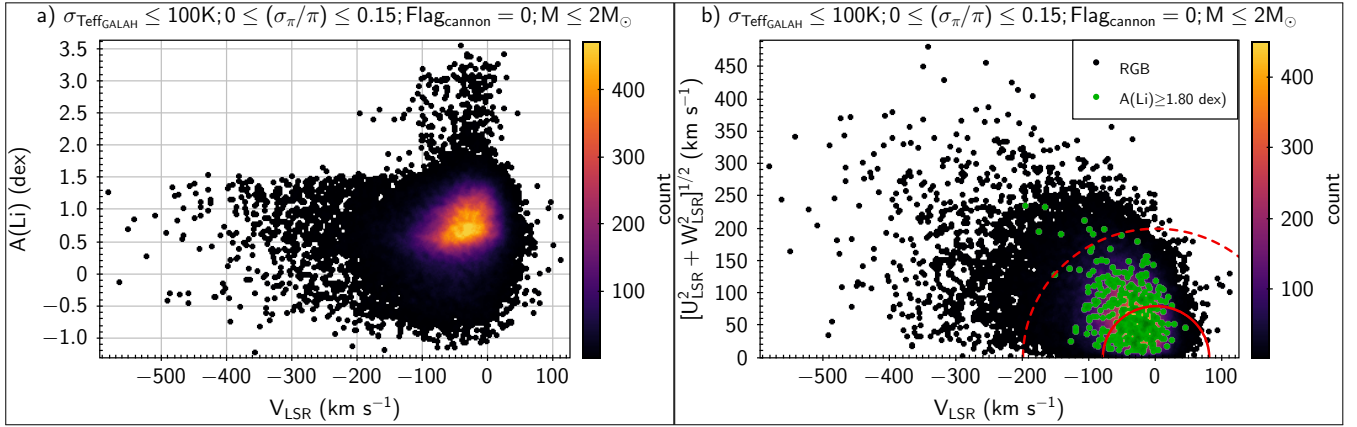


Figure 4. Distribution of selected RGB sample in $A(\text{Li})$ vs V_{LSR} plane and in the form of Toomre Diagram. In Figure-4b, we have plotted the approximate boundaries separating thin and think disk ($V_{\text{Total}}=80 \text{ km s}^{-1}$, continuous red circle), and thick disk and halo ($V_{\text{Total}}=200 \text{ km s}^{-1}$, dotted red circle).

giants that are below the bump luminosity about which we comment later.

4.3 Li-rich Giants in the Galaxy

To understand the distribution of Li-rich giants among different stellar components of the Galaxy, we have computed membership probability, based on the recipe given in Reddy et al. (2006) and references therein, for each of the stars in the selected RGB sample for belonging to one of the three main components of the Galaxy, namely; thin disk, thick disk and halo. For this, the heliocentric velocities (U, V, W) for each of the sample giant is calculated using the Gaia astrometry (positions, parallax, and proper motions) and radial velocities (RV) from the GALAH DR2. The heliocentric velocities are corrected for the solar motion using $U_o=10$, $V_o=5.3$, $W_o=7.2 \text{ (km s}^{-1}\text{)}$ from Dehnen & Binney (1998) to get velocities with respect to the local standard of rest ($U_{\text{LSR}}, V_{\text{LSR}}, W_{\text{LSR}}$). Entire sample is shown in Toomre Diagram of rotational velocity (V_{LSR}) and sum of quadrature of radial and vertical velocities ($[U_{\text{LSR}}^2 + W_{\text{LSR}}^2]^{1/2}$) (Sandage & Fouts 1987). Li-rich giants are identified by colored symbols as shown in Figure-4. We used kinematic boundaries for thin disk ($|V_{\text{Total}}| = [U_{\text{LSR}}^2 + V_{\text{LSR}}^2 + W_{\text{LSR}}^2]^{1/2} \leq 80 \text{ km s}^{-1}$), thick disk ($80 < |V_{\text{Total}}| \leq 200 \text{ km s}^{-1}$) and halo ($|V_{\text{Total}}| > 200 \text{ km s}^{-1}$) which are in accordance with the results in Reddy et al. (2006). Further to quantify the number of giants belonging to different components of the Galaxy, we used probability of 70% or more for any star being considered as a member of particular component. We found 223 Li-rich thin disk stars, which is about 0.8% of total thin disk RGB stars with $P_{\text{thin}} \geq 70\%$ and 69 Li-rich thick disk stars consisting of 0.5% of total thick disk RGB stars with $P_{\text{thick}} \geq 70\%$. We have found just 3 Li-rich giants among 1442 halo giants with $P_{\text{halo}} \geq 70\%$. This shows that Li-rich giants are rare (< 1%) across stellar components but are relatively more prevalent among metal-rich thin disk component compared to thick disk and very metal poor halo.

5 DISCUSSION

Surveys based on large pre-selected low mass RGB stars such as Kumar et al. (2011) and Smiljanic et al. (2018) using data from Hipparcos and *Gaia* catalogue respectively, suggested that Li-rich giants occupy a luminosity range in the HR diagram overlapping the luminosity of RC and RGB bump regions. This led to suggestions of internal nucleosynthesis as both the regions are associated with key phases of stellar evolution: removal of H-profile discontinuity and He-flash, respectively. There are observational reports suggesting existence of Li-rich stars before and after the luminosity bump on RGB, which indicates that Li-rich giants may occur anywhere on RGB, implying external origin for Li excess such as engulfment of sub-stellar objects. Now the question is whether the Li-rich giants happen anywhere along RGB or at a particular phase on RGB. Answer to this is a key to understand the origin of excess Li in RGB stars.

Thanks to the Kepler and CoRoT missions which provided wealth of time resolved photometric data for stars in certain fields of the sky. Using asteroseismic analysis, one can distinguish RGB giants of H-core burning from those of red clump giants of He-core burning (Bedding et al. 2011). Recently, half a dozen Li-rich giants which are in the Kepler fields haven been reported by different studies (Silva Aguirre et al. 2014; Bharat Kumar et al. 2018; Singh et al. 2019; Smiljanic et al. 2018). All of them have been classified as red clump stars with He-core burning based on asteroseismic data analysis with seismic parameters; average period spacing between g - and p -modes, $\Delta p \geq 150$ and frequency separation, $\Delta\nu \leq 5$. There is also a lone Li-rich giant (KIC 9821622) which is in Kepler field and has been classified as RGB star with H-core burning (Jofré et al. 2015). Values of luminosity and T_{eff} suggest its location below the luminosity bump on RGB. Though the star is a bona fide RGB, given its reported large difference in derived Li abundance between the stronger resonance line at 6707Å ($A(\text{Li})_{\text{LTE}} = 1.49 \text{ dex}$; $A(\text{Li})_{\text{NLTE}} = 1.65 \text{ dex}$) and weaker sub-ordinate line at 6103Å ($A(\text{Li})_{\text{LTE}} = 1.80 \text{ dex}$; $A(\text{Li})_{\text{NLTE}} = 1.94 \text{ dex}$), its status being Li-rich giant needs further studies. Also, star's average Li abundance of $(A(\text{Li}) = 1.80 \pm 0.2 \text{ dex}$ for

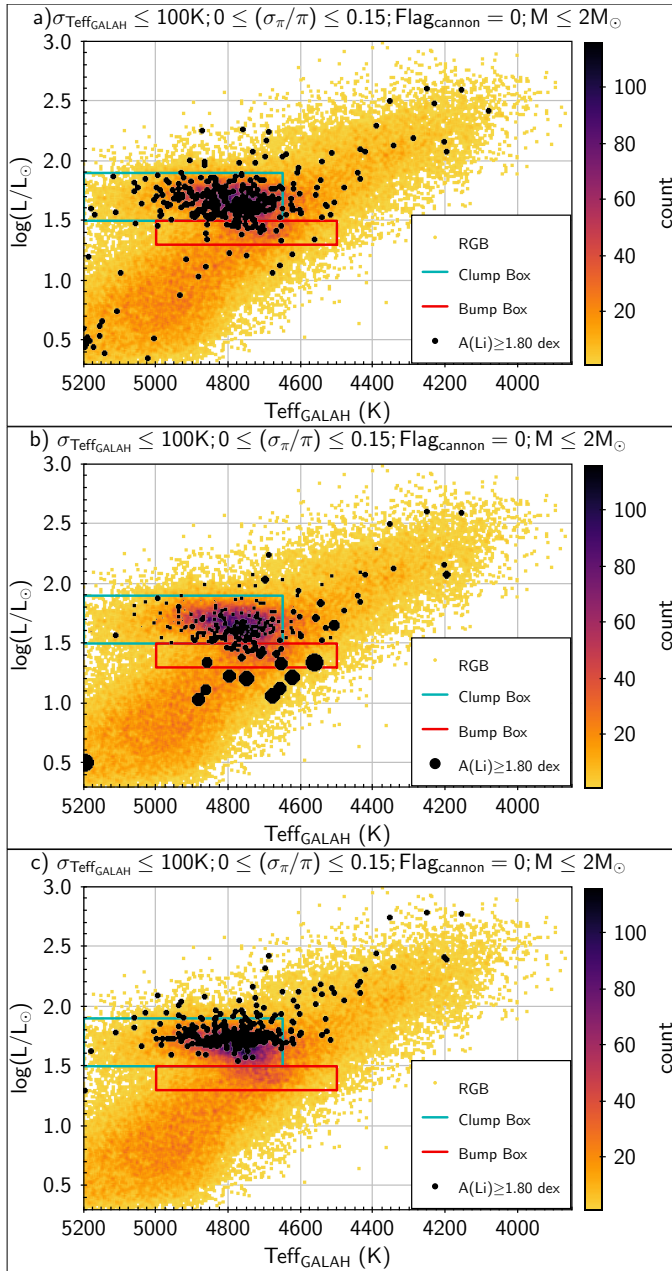


Figure 5. The HR diagram showing Li-rich giants’ positions a) prior to extinction correction, b) with size of representative point proportional to extinction, and c) post extinction correction.

a star with $[Fe/H] = -0.49 \pm 0.03$ dex) is at the border of the limit for Li-normal giants. However, in the absence of Kepler data for most of the known Li-rich stars and lack of systematic surveys for Li-rich giants among asteroseismically known RGB and RC stars, one cannot affirm that Li-rich stars belong only to RC region based on a small number of Li-rich stars randomly discovered. Large data set assembled here is quite suitable to find likely occurrence of Li-rich giants on different locations on RGB and possible origin mechanisms: external versus in-situ scenarios.

Table 1. Estimated evolutionary timescales for a representative $1M_{\odot}$ star with metallicities, $[Fe/H] = 0.0$ dex and -0.5 dex.

Evolutionary Phase	For $M=1M_{\odot}$ & $[Fe/H]=0$ dex	For $M=1M_{\odot}$ & $[Fe/H]=-0.5$ dex
	t_e (Gyr)	t_e (Gyr)
MS Turn-off to RGB tip	1.416	0.931
RGB base to tip	0.659	0.466
RGB base to Bump	0.555	0.402
RGB Bump	0.014	0.006
RGB Bump to RGB tip	0.100	0.059
He Core Burning	0.111	0.102

5.1 External versus in-situ Li enrichment

We examine external scenario of a planet or sub-stellar material accretion for excess Li in RGB stars. If this scenario has to hold, one would expect Li-rich giants across RGB with relatively higher concentration both at luminosity bump and red clump as their evolutionary timescales are relatively longer. In Table-1, we have given approximate evolutionary periods for different phases of RGB evolution for a representative $1M_{\odot}$ mass star of metallicity of $[Fe/H] = 0.0$ dex and -0.5 dex. Timescales are based on theoretical tracks taken from MESA Isochrones & Stellar Tracks’ latest version MISTv1.2 available at <http://waps.cfa.harvard.edu/MIST/index.html> and see Paxton et al. (2011) for more details. Evolutionary period for giants between base of RGB and tip of RGB is about 6 times more than that of evolutionary period of giants at the clumps which is about 110 Myrs. This means one should expect a number of Li-rich giants by a similar factor more on RGB in ascending phase including the bump compared to number of Li-rich giants at red clump region. Contrary to this, we found less than one third of the total Li-rich giants (about 106) outside the red clump box (see Figure-5a). Some of these, about 16, are lying just above the red clump box which probably are either evolving off red clump phase towards early AGB or descending from RGB tip. Quite a few (about 16) appear to be located below $L/L_{\odot} < 0.8$ dex, at the base of the RGB. Probably, these may still be in sub-giant phase and their higher Li abundance may be due to in-sufficient mixing as they might not have experienced fully the 1st dredge-up phase. In this context, we would like to mention the recent discovery of a number of metal-poor sub-giants with Li abundances $A(Li) \geq 2.0$ dex and in some cases exceeding ISM values (Li et al. 2018). There are also suggestions that Li excess seen in post 1st dredge-up on RGB giants probably originated from sub-giants (Kirby et al. 2016), though the origin of high Li in sub giants itself is not known yet.

Though the number of Li-rich stars on RGB are less, it is important to know if they are really on RGB in ascending phase or they are misplaced in the HR diagram due to errors. One of the errors that could be specific to individual giants is extinction, which can affect the stars’ brightness and hence its position in the HR diagram. In the present study, we have not taken into account the extinction in deriving luminosities, as the extinction values are not available

for majority of the sample stars. Moreover, the corrections for most of the stars in the sample are small as the stars are nearby ($d < 5$ kpc) bright giants (with $9 \leq m_v \leq 14$). However, on scrutiny of extinction among Li-rich giants, we found the extinction values only for 269 Li-rich giants out of 335. Interestingly, most of the Li-rich giants that are below the bump have relatively larger extinction values compared to others. In Figure 5b, for Li-rich giants with extinction values are shown. Level of extinction is represented by the size of the symbol. If we correct m_v values for extinction given in the Gaia DR2, many of the Li-rich giants that are below the bump on RGB move towards brighter clump box (Figure 5c). Some of them also moved out of the clump box towards higher luminosities. Particularly interesting is the fact that there are no Li-rich giants at the bump and also below the bump. Though it is compelling to suggest, based on the current data as shown in Figure 5c, that Li-rich giants belong only to RC, we note extinction has not been applied to the entire sample as it is not available for majority of the sample. One thing that emerges from Figure 5 is that large number of Li-rich giants seems to be at RC even though evolutionary period of RGB is many fold longer than RC giants.

In Table 2, we have separately given super Li-rich giants with $A(\text{Li}) \geq 3.2$ dex. There are 20 of them. Except one super Li-rich giant, all are closer to solar metallicity ($[\text{Fe}/\text{H}]$ within ± 0.30 dex and belongs to the Galactic thin disk. Super Li-rich giants are plotted in the HR diagram of Figure 6a. With the exemption of two, all falls in RC region defined by turquoise color box. Of two, one is below the bump and the second is above the clump region. Interestingly, the super Li-rich giant that appears below the bump has much larger extinction (larger the symbol higher the extinction) value as shown in Figure 6b. Post extinction correction, the lone super Li-rich giant below the bump moves up into red clump box. After extinction correction, super Li-rich giants seems to fall in the center of RC region as shown in Figure 6c. Two of the giants also move slightly upward towards brighter side away from the central region of RC. The giants above the clump are not RGB but are slightly leftwards. Probably, they are either post-clump giants evolving toward early AGB or post He-flash giants. Most importantly, none of the super Li-rich giants are either at bump or even on RGB. Given the transient nature of Li enrichment and very high Li abundance of super Li-rich giants, the Li enrichment, most probably, would have happened very recently. Clustering of super Li-rich stars only at the clump, as revealed by the data shown in Figure 6, is the most compelling evidence against external scenario for Li-excess origin. There is no reason to believe that the conditions for sub-stellar engulfment at RC are more favorable than at any other RGB phase. This clearly points towards in-situ scenario either at luminosity bump or its immediate preceding phase of He-flash at the RGB tip.

5.2 In-situ nucleosynthesis at luminosity bump versus He-flash

There are two likely phases at which nucleosynthesis and dredge-up of Li may happen: luminosity bump and He-flash at the RGB tip. Both the phases are associated with significant internal changes in the stars. It is at the bump at which

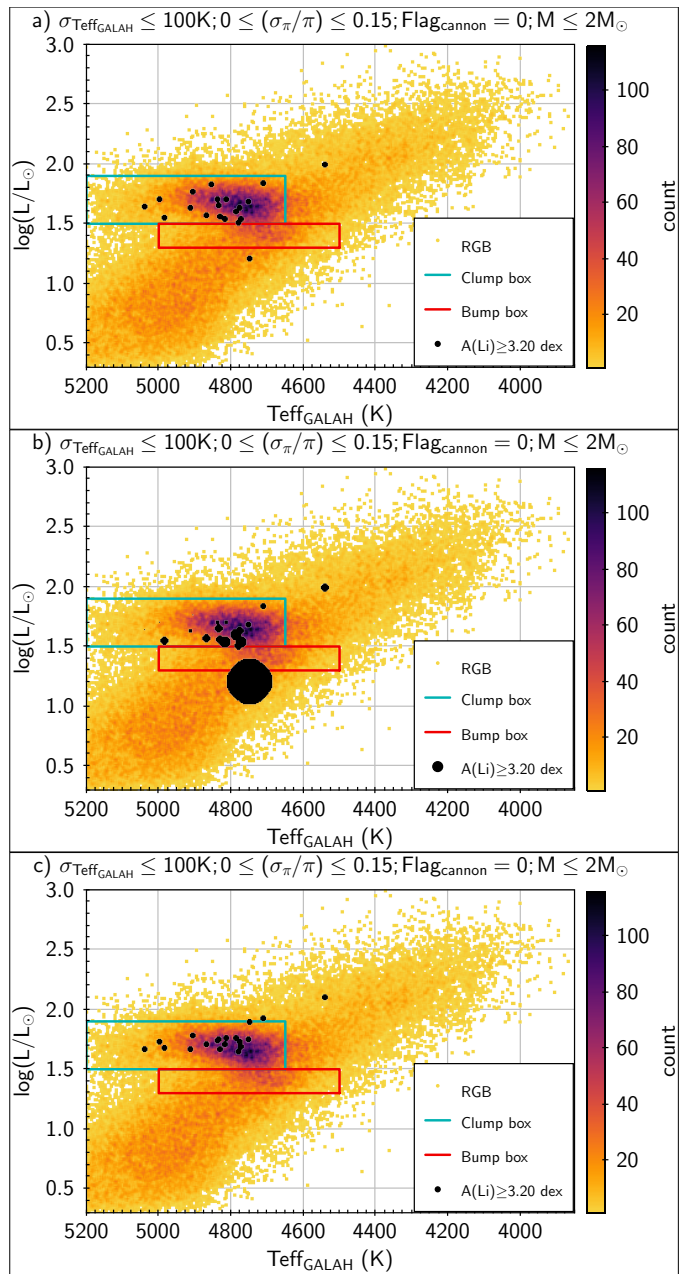


Figure 6. The HR diagram showing super Li-rich giants' positions a) prior to extinction correction, b) with size of representative point proportional to extinction, and c) post extinction correction.

H-burning shell moves upward and gets encroached by outer convective shell resulting in slowdown of stellar evolution which manifests as luminosity bump (Christensen-Dalsgaard 2015). Also, it is at the bump H-profile discontinuity, a barrier for convective mixing, which gets removed and resumes mixing up of $p-p$ -chain products with photosphere. Mixing at the bump, also known as extra-mixing, is attributed for rapid decrease in Li abundance and lowering of carbon isotopic ratios, $^{12}\text{C}/^{13}\text{C}$ (Gilroy 1989; Smiljanic et al. 2009). On the other hand, He-flash at the tip of RGB terminates RGB phase by removing electron degeneracy in the core (Iben & Renzini 1984). Post He-flash, stars settle at red clump qui-

Table 2. Stellar parameters of Super Li-rich giants with Li abundance of $A(\text{Li}) \geq 3.2$ dex in our sample.

S.No.	Object ID	Teff (K)	$\log g$ (dex)	[Fe/H] (dex)	m_v (mag)	L/L_\odot (dex)	$A(\text{Li})$ (dex)
1	Gaia DR2 6423511482552457344	4828.68 ± 58.32	2.84 ± 0.14	0.18 ± 0.05	12.15	1.56 ± 0.03	3.54 ± 0.12
2	Gaia DR2 6216747182780840576	4773.08 ± 58.40	2.69 ± 0.15	0.12 ± 0.06	12.54	1.54 ± 0.07	3.41 ± 0.12
3	Gaia DR2 3080569351805501824	4995.53 ± 95.89	2.60 ± 0.17	0.03 ± 0.07	11.07	1.71 ± 0.04	3.41 ± 0.12
4	Gaia DR2 5920543908525756800	4815.52 ± 76.34	2.68 ± 0.18	0.14 ± 0.07	11.71	1.54 ± 0.04	3.39 ± 0.13
5	Gaia DR2 5676420200792553600	4854.10 ± 97.57	2.31 ± 0.16	-0.11 ± 0.06	12.40	1.83 ± 0.07	3.38 ± 0.12
6	Gaia DR2 6721793108675117440	4911.04 ± 90.19	2.45 ± 0.17	-0.04 ± 0.07	11.36	1.64 ± 0.04	3.33 ± 0.12
7	Gaia DR2 4488063566731544960	4778.94 ± 86.05	2.37 ± 0.16	-0.02 ± 0.06	12.34	1.52 ± 0.05	3.27 ± 0.12
8	Gaia DR2 2939800046333110272	4985.20 ± 83.68	2.56 ± 0.18	-0.13 ± 0.08	12.98	1.55 ± 0.06	3.26 ± 0.13
9	Gaia DR2 4168437628181576192	4749.88 ± 89.58	2.71 ± 0.18	0.19 ± 0.07	13.23	1.21 ± 0.06	3.26 ± 0.13
10	Gaia DR2 5229729170925959552	5038.38 ± 70.89	2.79 ± 0.17	-0.15 ± 0.07	11.13	1.65 ± 0.02	3.24 ± 0.13
11	Gaia DR2 5293680581122445184	4832.25 ± 68.88	2.50 ± 0.15	-0.01 ± 0.06	12.68	1.65 ± 0.04	3.23 ± 0.12
12	Gaia DR2 5242382659974594688	4786.39 ± 51.84	2.80 ± 0.14	0.28 ± 0.05	11.57	1.60 ± 0.03	3.23 ± 0.12
13	Gaia DR2 6721685773156936064	4751.60 ± 58.24	2.52 ± 0.15	0.11 ± 0.06	10.87	1.68 ± 0.04	3.23 ± 0.12
14	Gaia DR2 5628302754467688576	4868.94 ± 93.16	2.37 ± 0.17	-0.20 ± 0.07	13.47	1.57 ± 0.04	3.21 ± 0.13
15	Gaia DR2 3202012502737830784	4906.32 ± 86.59	2.42 ± 0.16	-0.14 ± 0.06	12.78	1.77 ± 0.11	3.21 ± 0.12
16	Gaia DR2 5460011229840058880	4813.14 ± 50.93	2.63 ± 0.13	0.16 ± 0.05	12.17	1.70 ± 0.05	3.21 ± 0.12
17	Gaia DR2 5452473905831060480	4711.60 ± 70.91	2.17 ± 0.15	-0.30 ± 0.06	12.41	1.84 ± 0.07	3.20 ± 0.12
18	Gaia DR2 6162898261508964992	4835.99 ± 77.44	2.58 ± 0.17	0.01 ± 0.07	12.59	1.70 ± 0.12	3.20 ± 0.13
19	Gaia DR2 6779302244026689920	4541.30 ± 69.25	2.17 ± 0.15	-0.48 ± 0.06	12.02	1.99 ± 0.08	3.20 ± 0.12
20	Gaia DR2 3496188144418768640	4776.14 ± 72.41	2.59 ± 0.16	0.04 ± 0.06	12.12	1.63 ± 0.05	3.20 ± 0.12

escently burning He at the core with outer H-burning shell before climbing up towards AGB.

There are a number of theoretical models dealing with extra mixing at the bump (Eggleton et al. 2008; Charbonnel & Lagarde 2010; Denissenkov & Merryfield 2011; Denissenkov 2012). The models do suggest synthesis of Li via Cameron-Fowler mechanism in H-shell and somehow dredge-up with photosphere. The models were invoked with the presumption that Li-rich giants occur at the bump as reported by many observational studies (Charbonnel & Balachandran 2000; Kumar et al. 2011; Yan et al. 2018). However, it is not clear how the same mechanism that is responsible for rapid depletion of Li is also responsible for Li enhancement. The lack of clarity on Li origin probably stems from the fact that evolutionary phase of Li-rich giants has not been identified without ambiguity. The reported Li-rich giants fall in a narrow luminosity range which overlaps both bump and clump regions. Difference between clump and bump values of luminosity and T_{eff} are small, and many a times, they are within the measured uncertainties. This degeneracy even led to the suggestion that Li-rich giants may make zigzag motion and appear as clump or bump due to internal rotation (Denissenkov 2012). Let us tackle this issue using this large data set and evolutionary period argument, as it requires a large number of stars to define the luminosity bump.

Among 335 Li-rich giants, there are only 106 giants which appear outside the red clump. Only one third of these seem to be either at the bump or above the bump. The large concentration of Li-rich giants at RC suggests, probably, that the origin of Li enhancement lies at or post He-flash rather than at the luminosity bump. If Li enhancement occurred at the bump, the enhanced Li has to be sustained till RC which is quite unlikely given the deep convection post bump evolution. One would also expect significant number of Li-rich giants both at the bump and between bump and the RGB tip, because the evolutionary periods (see Table-1)

of giants between the bump to RGB tip (100 Myrs) and the red clump (100 Myrs) are similar. This is not the case as shown in Figure-4, as there is a factor of about four more Li-rich giants at the clump compared to those at the bump or post-bump evolution. One could make another argument against the bump as the site for Li origin based on very short Li depletion periods compared to evolutionary time of luminosity bump (see Palacios et al. 2001; Bharat Kumar et al. 2015). The enhanced Li may deplete within 60% of the evolutionary period of the bump, i.e Li-rich giants may become Li-normal within a few million years which is much shorter than the evolutionary periods between the bump and RC. Based on this argument, it is reasonable to suggest that all the Li-rich giants are, most likely, in He-core burning phase rather than at multiple phases on RGB for Li origin. Of course, we need to have further studies to understand a minority of Li-rich giants that are outside of the RC region. This conclusion is also strengthened by the fact that all the presently known six Li-rich giants (e.g., Singh et al. 2019) that are in Kepler field are red clump giants. Data assembled in Figure-5 and Figure-6 suggests that most of the Li-rich giants are at red clump which implicitly points towards He-flash, a major stellar event preceding red clump, for Li enrichment. However, we do not have much insight into the nucleosynthesis and dredge-up processes during He-flash, except a couple of studies to understand Li-rich giants at the red clump or the early AGB stars of J-type. For example, the study Mocák et al. (2011) deals with Li production during He-flash, but in case of very metal-poor giants. They show that the requirement of proton injection into the convective shell powered by He burning during He flash may not be met in the case of metal-rich giants as He-ignition occurs relatively farther away from the H-burning shell. For explaining large Li abundances in J-type stars, Zhang & Jeffery (2013) explored merging up of He white dwarfs (WDs) of different

masses with the He-core of RGB giants and showed that they could produce observed values for certain combinations.

6 CONCLUSION

In this paper, we have searched for Li-rich giants among a large data set of red giant branch stars given in the GALAH catalogue for which the Gaia astrometry is available. We found 335 giants with $A(\text{Li}) \geq 1.80$ dex, an abundance which is more than the maximum Li abundance expected from canonical stellar models for stars in the mass range of 1 to $1.5M_{\odot}$. Among these, we found 20 super Li-rich giants with $A(\text{Li}) \geq 3.20$ dex. This is the largest number of Li-rich giants ever reported in a single study. Values of Luminosity based on the Gaia parallax and T_{eff} given in the GALAH suggest that majority of the Li-rich giants are red clump giants as defined in the HR diagram. Only a minority of them are outside it. About a dozen of Li-rich giants are found below the bump which may be sub-giants. The high Li in them may be due to insufficient mixing and dilution from its initial values. There are a couple of Li-rich giants which are above RC and leftwards of RGB, which may either be evolving off the red clump or just on their way to RC after experiencing He-flash at the RGB tip. A few Li-rich giants that seem to fall in the bump region as defined in the HR diagram needs to be studied further.

With the advantage of large data set with well defined evolutionary phases on RGB, we addressed the key issue of origin scenarios: external accretion versus in-situ nucleosynthesis. If the cause for Li excess is due to external accretion, one would expect Li-rich giants across RGB. However, disproportionately large concentration of Li-rich giants at a single evolutionary phase of red clump compared to those on RGB phase, between RGB base and its tip, suggest that external origin for Li enrichment is an unlikely scenario. Though the large data set provides compelling evidence that Li-rich giants may belong to RC with He-core burning phase, we cannot dismiss the possibility of a few Li rich giants on other phases on RGB with different sources of Li enhancement. To firmly establish whether there is single or multiple sites on RGB for Li origin, it is important to conduct further studies such as asteroseismic analysis and detailed abundance studies of all the known Li-rich giants.

ACKNOWLEDGMENTS

This work has made use of data from the European Space Agency (ESA) mission *Gaia* (<https://www.cosmos.esa.int/gaia>), processed by the *Gaia* Data Processing and Analysis Consortium (DPAC, <https://www.cosmos.esa.int/web/gaia/dpac/consortium>). Funding for the DPAC has been provided by national institutions, in particular the institutions participating in the *Gaia* Multilateral Agreement. This work has also made use of the GALAH survey which includes data acquired through the Australian Astronomical Observatory. In addition, authors thank Raghubar Singh for his help with stellar evolutionary tracks, and the anonymous reviewers for their constructive comments and suggestions, which helped us to improve the manuscript.

ORCID IDS

Deepak: <https://orcid.org/0000-0003-2048-9870>
 B. E. Reddy: <https://orcid.org/0000-0001-9246-9743>

REFERENCES

- Aguilera-Gómez C., Chanamé J., Pinsonneault M. H., Carlberg J. K., 2016, *ApJ*, **833**, L24
 Andrae R., et al., 2018, *A&A*, **616**, A8
 Bedding T. R., et al., 2011, *Nature*, **471**, 608
 Bharat Kumar Y., Reddy B. E., Muthumariappan C., Zhao G., 2015, *A&A*, **577**, A10
 Bharat Kumar Y., Singh R., Eswar Reddy B., Zhao G., 2018, *ApJ*, **858**, L22
 Brown J. A., Sneden C., Lambert D. L., Dutchover Jr. E., 1989, *ApJS*, **71**, 293
 Buder S., et al., 2018, *MNRAS*, **478**, 4513
 Cameron A. G. W., Fowler W. A., 1971, *ApJ*, **164**, 111
 Carlberg J. K., Cunha K., Smith V. V., 2016, *ApJ*, **827**, 129
 Casey A. R., et al., 2016, *MNRAS*, **461**, 3336
 Cassisi S., Salaris M., Pietrinferni A., 2016, *A&A*, **585**, A124
 Charbonnel C., Balachandran S. C., 2000, *A&A*, **359**, 563
 Charbonnel C., Lagarde N., 2010, *A&A*, **522**, A10
 Christensen-Dalsgaard J., 2015, *MNRAS*, **453**, 666
 Cyburt R. H., Fields B. D., Olive K. A., 2008, *J. Cosmology Astropart. Phys.*, **11**, 012
 Dehnen W., Binney J. J., 1998, *MNRAS*, **298**, 387
 Deliyannis C. P., 1990, PhD thesis, Yale University, New Haven, CT.
 Denissenkov P. A., 2012, *ApJ*, **753**, L3
 Denissenkov P. A., Merryfield W. J., 2011, *ApJ*, **727**, L8
 Eggleton P. P., Dearborn D. S. P., Lattanzio J. C., 2008, *ApJ*, **677**, 581
 Fields B. D., 2011, *Annual Review of Nuclear and Particle Science*, **61**, 47
 Gaia Collaboration et al., 2018, *A&A*, **616**, A1
 Gilroy K. K., 1989, *ApJ*, **347**, 835
 Iben Jr. I., 1967, *ApJ*, **147**, 624
 Iben I., Renzini A., 1984, *Phys. Rep.*, **105**, 329
 Izzo L., et al., 2015, *ApJ*, **808**, L14
 Jofré E., Petrucci R., García L., Gómez M., 2015, *A&A*, **584**, L3
 Kirby E. N., Fu X., Guhathakurta P., Deng L., 2012, *ApJ*, **752**, L16
 Kirby E. N., Guhathakurta P., Zhang A. J., Hong J., Guo M., Guo R., Cohen J. G., Cunha K., 2016, *ApJ*, **819**, 135
 Kumar Y. B., Reddy B. E., Lambert D. L., 2011, *ApJ*, **730**, L12
 Lambert D. L., Reddy B. E., 2004, *MNRAS*, **349**, 757
 Lattanzio J., Frost C., Cannon R., Wood P. R., 1996, *Mem. Soc. Astron. Italiana*, **67**, 729
 Li H., Aoki W., Matsuno T., Bharat Kumar Y., Shi J., Suda T., Zhao G., 2018, *ApJ*, **852**, L31
 Mitler H. E., 1972, *Ap&SS*, **17**, 186
 Mocák M., Meakin C. A., Müller E., Siess L., 2011, *ApJ*, **743**, 55
 Mowlavi N., 1995, in Crane P., ed., *The Light Element Abundances*. p. 297
 Palacios A., Charbonnel C., Forestini M., 2001, *A&A*, **375**, L9
 Paxton B., Bildsten L., Dotter A., Herwig F., Lesaffre P., Timmes F., 2011, *ApJS*, **192**, 3
 Reddy B. E., Lambert D. L., Allende Prieto C., 2006, *MNRAS*, **367**, 1329
 Salaris M., Cassisi S., Weiss A., 2002, *PASP*, **114**, 375
 Sandage A., Fouts G., 1987, *AJ*, **93**, 74
 Silva Aguirre V., et al., 2014, *ApJ*, **784**, L16
 Singh R., Reddy B. E., Kumar Y. B., 2019, *MNRAS*, **482**, 3822
 Smiljanic R., Gauderon R., North P., Barbuy B., Charbonnel C., Mowlavi N., 2009, *A&A*, **502**, 267

- Smiljanic R., et al., 2016, [A&A](#), **591**, A62
Smiljanic R., et al., 2018, [A&A](#), **617**, A4
Smith V. V., Lambert D. L., 1989, [ApJ](#), **345**, L75
Tajitsu A., Sadakane K., Naito H., Arai A., Aoki W., 2015, [Nature](#), **518**, 381
Ting Y.-S., Hawkins K., Rix H.-W., 2018, [ApJ](#), **858**, L7
Vrard M., Mosser B., Samadi R., 2016, [A&A](#), **588**, A87
Wallerstein G., Sneden C., 1982, [ApJ](#), **255**, 577
Yan H.-L., et al., 2018, [Nature Astronomy](#), **2**, 790
Zhang X., Jeffery C. S., 2013, [MNRAS](#), **430**, 2113

This paper has been typeset from a T_EX/L^AT_EX file prepared by the author.

Table 3. Stellar parameters of Li-rich giants with Li abundance of $A(\text{Li}) \geq 1.8$ dex in our sample. (Supplementary table will be available online.)

S.No.	Object ID	Teff (K)	$\log g$ (dex)	[Fe/H] (dex)	m_v (mag)	L/L_\odot (dex)	$A(\text{Li})$ (dex)
1	Gaia DR2 6423511482552457344	4828.68 ± 58.32	2.84 ± 0.14	0.18 ± 0.05	12.15	1.56 ± 0.03	3.54 ± 0.12
2	Gaia DR2 6216747182780840576	4773.08 ± 58.40	2.69 ± 0.15	0.12 ± 0.06	12.54	1.54 ± 0.07	3.41 ± 0.12
3	Gaia DR2 3080569351805501824	4995.53 ± 95.89	2.60 ± 0.17	0.03 ± 0.07	11.07	1.71 ± 0.04	3.41 ± 0.12
4	Gaia DR2 5920543908525756800	4815.52 ± 76.34	2.68 ± 0.18	0.14 ± 0.07	11.71	1.54 ± 0.04	3.39 ± 0.13
5	Gaia DR2 5676420200792553600	4854.10 ± 97.57	2.31 ± 0.16	-0.11 ± 0.06	12.40	1.83 ± 0.07	3.38 ± 0.12
6	Gaia DR2 6721793108675117440	4911.04 ± 90.19	2.45 ± 0.17	-0.04 ± 0.07	11.36	1.64 ± 0.04	3.33 ± 0.12
7	Gaia DR2 4488063566731544960	4778.94 ± 86.05	2.37 ± 0.16	-0.02 ± 0.06	12.34	1.52 ± 0.05	3.27 ± 0.12
8	Gaia DR2 2939800046333110272	4985.20 ± 83.68	2.56 ± 0.18	-0.13 ± 0.08	12.98	1.55 ± 0.06	3.26 ± 0.13
9	Gaia DR2 4168437628181576192	4749.88 ± 89.58	2.71 ± 0.18	0.19 ± 0.07	13.23	1.21 ± 0.06	3.26 ± 0.13
10	Gaia DR2 5229729170925959552	5038.38 ± 70.89	2.79 ± 0.17	-0.15 ± 0.07	11.13	1.65 ± 0.02	3.24 ± 0.13
11	Gaia DR2 5293680581122445184	4832.25 ± 68.88	2.50 ± 0.15	-0.01 ± 0.06	12.68	1.65 ± 0.04	3.23 ± 0.12
12	Gaia DR2 5242382659974594688	4786.39 ± 51.84	2.80 ± 0.14	0.28 ± 0.05	11.57	1.60 ± 0.03	3.23 ± 0.12
13	Gaia DR2 6721685773156936064	4751.60 ± 58.24	2.52 ± 0.15	0.11 ± 0.06	10.87	1.68 ± 0.04	3.23 ± 0.12
14	Gaia DR2 5628302754467688576	4868.94 ± 93.16	2.37 ± 0.17	-0.20 ± 0.07	13.47	1.57 ± 0.04	3.21 ± 0.13
15	Gaia DR2 3202012502737830784	4906.32 ± 86.59	2.42 ± 0.16	-0.14 ± 0.06	12.78	1.77 ± 0.11	3.21 ± 0.12
16	Gaia DR2 5460011229840058880	4813.14 ± 50.93	2.63 ± 0.13	0.16 ± 0.05	12.17	1.70 ± 0.05	3.21 ± 0.12
17	Gaia DR2 5452473905831060480	4711.60 ± 70.91	2.17 ± 0.15	-0.30 ± 0.06	12.41	1.84 ± 0.07	3.20 ± 0.12
18	Gaia DR2 6162898261508964992	4835.99 ± 77.44	2.58 ± 0.17	0.01 ± 0.07	12.59	1.70 ± 0.12	3.20 ± 0.13
19	Gaia DR2 6779302244026689920	4541.30 ± 69.25	2.17 ± 0.15	-0.48 ± 0.06	12.02	1.99 ± 0.08	3.20 ± 0.12
20	Gaia DR2 3496188144418768640	4776.14 ± 72.41	2.59 ± 0.16	0.04 ± 0.06	12.12	1.63 ± 0.05	3.20 ± 0.12
21	Gaia DR2 5446401096954011264	4834.50 ± 77.10	2.27 ± 0.16	-0.24 ± 0.06	13.33	1.86 ± 0.08	3.18 ± 0.12
22	Gaia DR2 5380617896081668608	4936.61 ± 82.12	2.32 ± 0.17	-0.26 ± 0.07	12.95	1.77 ± 0.09	3.18 ± 0.12
23	Gaia DR2 5467139329361254144	4683.37 ± 76.26	2.54 ± 0.17	0.20 ± 0.07	12.96	1.66 ± 0.07	3.15 ± 0.13
24	Gaia DR2 5819295071037261824	4837.62 ± 95.07	2.60 ± 0.18	0.06 ± 0.08	11.96	1.60 ± 0.03	3.10 ± 0.13
25	Gaia DR2 6385336541913936512	4738.25 ± 82.88	1.89 ± 0.16	-0.59 ± 0.06	12.28	1.84 ± 0.05	3.09 ± 0.12
26	Gaia DR2 6204948465240692736	4791.82 ± 63.13	2.66 ± 0.17	0.15 ± 0.07	12.62	1.62 ± 0.07	3.09 ± 0.12
27	Gaia DR2 5779908846543414016	4806.52 ± 66.85	2.56 ± 0.17	0.02 ± 0.07	12.42	1.54 ± 0.04	3.09 ± 0.12
28	Gaia DR2 4140059031209507456	4677.78 ± 66.24	3.07 ± 0.17	0.47 ± 0.07	12.97	1.07 ± 0.04	3.08 ± 0.13
29	Gaia DR2 6093873292346168064	4802.64 ± 79.08	2.45 ± 0.19	0.05 ± 0.08	11.33	1.47 ± 0.06	3.08 ± 0.13
30	Gaia DR2 6845853685693093504	4904.20 ± 95.05	2.16 ± 0.18	-0.38 ± 0.07	12.23	2.01 ± 0.09	3.07 ± 0.13
31	Gaia DR2 5623835163845080576	4821.88 ± 65.10	2.62 ± 0.17	0.15 ± 0.07	11.63	1.56 ± 0.03	3.07 ± 0.13
32	Gaia DR2 5907710473221745152	4797.55 ± 82.93	2.50 ± 0.19	0.10 ± 0.08	12.24	1.74 ± 0.06	3.06 ± 0.13
33	Gaia DR2 4248247505054982144	4897.40 ± 93.05	2.82 ± 0.21	0.21 ± 0.09	11.31	1.56 ± 0.05	3.06 ± 0.14
34	Gaia DR2 5776389997014959232	4545.21 ± 94.95	2.13 ± 0.19	-0.42 ± 0.08	13.82	1.84 ± 0.06	3.05 ± 0.13
35	Gaia DR2 5421808423456535936	4838.15 ± 96.19	2.38 ± 0.18	-0.13 ± 0.07	12.55	1.86 ± 0.06	3.05 ± 0.13
36	Gaia DR2 543342554977634304	4888.15 ± 92.06	2.53 ± 0.18	-0.12 ± 0.08	12.60	1.69 ± 0.05	3.05 ± 0.13
37	Gaia DR2 6093817968865392768	5177.02 ± 83.79	2.82 ± 0.19	-0.22 ± 0.08	12.46	1.60 ± 0.09	3.05 ± 0.13
38	Gaia DR2 6188759423532409472	4674.71 ± 64.71	2.60 ± 0.16	0.16 ± 0.06	12.45	1.62 ± 0.05	3.05 ± 0.12
39	Gaia DR2 5908117846580723328	4602.58 ± 87.89	2.11 ± 0.18	-0.13 ± 0.07	11.18	1.73 ± 0.03	3.05 ± 0.13
40	Gaia DR2 6703523455968541568	4658.06 ± 86.01	2.63 ± 0.19	0.19 ± 0.08	13.57	1.69 ± 0.08	3.04 ± 0.13
41	Gaia DR2 6892346397434608384	4698.31 ± 80.33	2.49 ± 0.18	0.04 ± 0.07	12.68	1.67 ± 0.07	3.04 ± 0.13
42	Gaia DR2 6715209443503275776	4679.61 ± 84.15	2.31 ± 0.16	-0.14 ± 0.06	11.20	1.77 ± 0.06	3.04 ± 0.12
43	Gaia DR2 6014097882591550976	4761.92 ± 88.93	2.31 ± 0.17	-0.25 ± 0.07	13.57	1.39 ± 0.06	3.03 ± 0.13
44	Gaia DR2 5819154642796257664	4702.46 ± 77.61	2.84 ± 0.20	0.32 ± 0.08	11.52	1.46 ± 0.03	3.03 ± 0.14
45	Gaia DR2 5821626207499355392	4772.56 ± 76.32	2.63 ± 0.19	0.12 ± 0.08	11.43	1.45 ± 0.03	3.03 ± 0.13
46	Gaia DR2 5634364362072360064	4716.95 ± 87.81	2.61 ± 0.19	0.08 ± 0.08	13.63	1.57 ± 0.05	3.02 ± 0.13
47	Gaia DR2 6087493341765160576	5183.81 ± 70.54	3.32 ± 0.19	0.23 ± 0.08	13.94	1.20 ± 0.06	3.02 ± 0.13
48	Gaia DR2 6566057220857377664	4701.72 ± 85.32	2.10 ± 0.19	-0.47 ± 0.08	12.21	1.71 ± 0.09	3.02 ± 0.13
49	Gaia DR2 6130099825359747584	4783.58 ± 55.53	2.77 ± 0.15	0.25 ± 0.06	12.14	1.62 ± 0.05	3.02 ± 0.12
50	Gaia DR2 5380837493466374272	4781.18 ± 56.09	2.89 ± 0.16	0.39 ± 0.06	12.46	1.49 ± 0.04	3.02 ± 0.12
51	Gaia DR2 6705449899116253312	4883.28 ± 76.61	2.38 ± 0.19	-0.11 ± 0.08	11.96	1.58 ± 0.06	3.02 ± 0.13
52	Gaia DR2 5229986692861011200	4830.59 ± 76.71	2.62 ± 0.18	-0.03 ± 0.07	13.31	1.67 ± 0.04	3.01 ± 0.13
53	Gaia DR2 5703002509304050944	4738.37 ± 79.54	2.41 ± 0.16	-0.15 ± 0.07	12.98	1.77 ± 0.08	3.01 ± 0.12
54	Gaia DR2 5414135481563472640	4744.30 ± 55.03	2.72 ± 0.16	0.25 ± 0.06	11.62	1.65 ± 0.04	3.01 ± 0.12
55	Gaia DR2 2898121301434595584	4815.25 ± 67.73	2.39 ± 0.15	-0.14 ± 0.06	12.17	1.71 ± 0.04	3.00 ± 0.12
56	Gaia DR2 5294650522177685120	4845.01 ± 65.21	2.55 ± 0.15	-0.08 ± 0.06	12.82	1.52 ± 0.03	2.98 ± 0.12
57	Gaia DR2 5823358488074533120	4965.30 ± 96.45	2.51 ± 0.20	-0.01 ± 0.08	12.14	1.64 ± 0.04	2.97 ± 0.14
58	Gaia DR2 5947597289051638784	4763.65 ± 80.92	2.35 ± 0.18	-0.07 ± 0.07	12.12	1.65 ± 0.06	2.97 ± 0.13
59	Gaia DR2 6088362363965385216	4862.10 ± 55.61	2.42 ± 0.13	-0.06 ± 0.05	12.48	1.65 ± 0.07	2.96 ± 0.12
60	Gaia DR2 5572621698926229120	4802.91 ± 85.70	2.36 ± 0.17	-0.14 ± 0.07	13.21	1.66 ± 0.04	2.95 ± 0.13

Table 3 – continued

S.No.	Object ID	Teff (K)	$\log g$ (dex)	[Fe/H] (dex)	m_v (mag)	L/L_\odot (dex)	A(Li) (dex)
61	Gaia DR2 6661697548308365312	4660.75 ± 60.36	2.46 ± 0.17	0.09 ± 0.07	12.43	1.68 ± 0.09	2.95 ± 0.12
62	Gaia DR2 4242037738259542784	4864.57 ± 79.32	2.35 ± 0.18	-0.06 ± 0.07	11.94	1.63 ± 0.05	2.95 ± 0.13
63	Gaia DR2 5204530013679857280	4892.15 ± 88.58	2.40 ± 0.18	-0.16 ± 0.07	13.24	1.54 ± 0.04	2.93 ± 0.13
64	Gaia DR2 5921483333826980224	4809.35 ± 55.37	2.40 ± 0.12	-0.09 ± 0.05	12.12	1.58 ± 0.06	2.93 ± 0.11
65	Gaia DR2 5468677168171016320	4718.90 ± 54.08	2.48 ± 0.14	-0.11 ± 0.05	12.26	1.75 ± 0.06	2.92 ± 0.12
66	Gaia DR2 5814033255067021312	4342.28 ± 91.66	1.56 ± 0.19	-0.50 ± 0.08	12.64	2.13 ± 0.13	2.91 ± 0.13
67	Gaia DR2 5702810159189857408	4730.05 ± 72.93	2.32 ± 0.16	-0.02 ± 0.06	13.05	1.51 ± 0.07	2.91 ± 0.12
68	Gaia DR2 5793668547375510016	4759.90 ± 66.51	2.13 ± 0.17	0.00 ± 0.07	11.13	2.26 ± 0.04	2.91 ± 0.13
69	Gaia DR2 5246928075402201216	4598.41 ± 60.79	2.73 ± 0.17	0.26 ± 0.07	11.39	1.56 ± 0.02	2.91 ± 0.12
70	Gaia DR2 3135783149258877824	4917.72 ± 63.69	2.27 ± 0.16	-0.55 ± 0.06	12.61	1.78 ± 0.08	2.89 ± 0.12
71	Gaia DR2 6008102726729861632	4880.12 ± 92.64	2.87 ± 0.19	0.13 ± 0.08	13.57	1.04 ± 0.35	2.89 ± 0.13
72	Gaia DR2 2679552786563683328	4668.91 ± 71.58	2.31 ± 0.16	-0.13 ± 0.06	12.91	1.77 ± 0.10	2.88 ± 0.12
73	Gaia DR2 6736616969290744576	4789.81 ± 68.49	2.56 ± 0.17	0.13 ± 0.07	10.91	1.60 ± 0.05	2.88 ± 0.12
74	Gaia DR2 6688605041679237248	4887.88 ± 69.33	2.36 ± 0.16	-0.32 ± 0.06	12.59	1.68 ± 0.07	2.86 ± 0.12
75	Gaia DR2 4486423365960888192	4731.80 ± 45.68	2.28 ± 0.11	-0.15 ± 0.04	11.92	1.60 ± 0.04	2.86 ± 0.11
76	Gaia DR2 5371457559771370368	4809.21 ± 60.44	2.65 ± 0.17	0.16 ± 0.07	11.51	1.66 ± 0.06	2.86 ± 0.12
77	Gaia DR2 6735047343387113088	4736.17 ± 87.03	2.78 ± 0.19	0.20 ± 0.08	13.41	1.58 ± 0.06	2.85 ± 0.13
78	Gaia DR2 6094984761160506240	5057.13 ± 55.82	2.75 ± 0.15	-0.12 ± 0.06	10.73	1.75 ± 0.05	2.85 ± 0.12
79	Gaia DR2 6082878897620910336	4832.60 ± 85.91	2.73 ± 0.19	0.22 ± 0.08	10.66	1.66 ± 0.07	2.85 ± 0.13
80	Gaia DR2 6654103668171738880	4867.99 ± 68.80	2.53 ± 0.16	-0.07 ± 0.07	12.67	1.73 ± 0.07	2.84 ± 0.12
81	Gaia DR2 6134488083643500928	4842.17 ± 58.42	2.47 ± 0.15	-0.06 ± 0.06	12.28	1.67 ± 0.07	2.84 ± 0.12
82	Gaia DR2 5661751169489845760	4759.45 ± 76.23	2.11 ± 0.17	-0.34 ± 0.07	13.19	1.71 ± 0.13	2.82 ± 0.13
83	Gaia DR2 5790803112691487232	4712.54 ± 68.05	2.64 ± 0.17	0.28 ± 0.07	13.81	1.44 ± 0.04	2.82 ± 0.13
84	Gaia DR2 5367726126545882240	4436.05 ± 59.71	2.18 ± 0.16	-0.16 ± 0.06	11.36	2.10 ± 0.04	2.82 ± 0.12
85	Gaia DR2 4359923561049343744	4652.36 ± 77.52	2.96 ± 0.21	0.39 ± 0.09	13.33	1.33 ± 0.07	2.82 ± 0.14
86	Gaia DR2 4904707520793305216	4730.07 ± 90.88	2.31 ± 0.19	-0.19 ± 0.08	12.96	1.71 ± 0.06	2.80 ± 0.13
87	Gaia DR2 5470340896766060800	4752.70 ± 73.82	2.62 ± 0.19	0.20 ± 0.08	12.87	1.63 ± 0.08	2.78 ± 0.13
88	Gaia DR2 6454923636405184640	4835.79 ± 74.53	2.18 ± 0.17	-0.49 ± 0.07	12.68	1.67 ± 0.05	2.77 ± 0.13
89	Gaia DR2 5791378917488589952	4730.86 ± 94.21	2.39 ± 0.18	-0.03 ± 0.07	12.92	1.45 ± 0.05	2.77 ± 0.13
90	Gaia DR2 6108301045262477952	4842.90 ± 84.12	2.31 ± 0.19	-0.07 ± 0.08	11.86	1.69 ± 0.07	2.77 ± 0.13
91	Gaia DR2 6129782620559721344	4774.26 ± 55.89	2.63 ± 0.16	0.14 ± 0.06	10.75	1.68 ± 0.02	2.77 ± 0.12
92	Gaia DR2 3200477756303359616	5154.93 ± 58.30	3.67 ± 0.17	0.06 ± 0.07	12.40	0.63 ± 0.02	2.77 ± 0.12
93	Gaia DR2 6145981622281078912	4886.66 ± 84.32	2.36 ± 0.17	-0.16 ± 0.07	13.29	1.70 ± 0.10	2.76 ± 0.13
94	Gaia DR2 4200949362381698944	4809.22 ± 85.59	2.55 ± 0.19	0.04 ± 0.08	13.27	1.56 ± 0.11	2.76 ± 0.13
95	Gaia DR2 5702816893698573952	4975.65 ± 59.50	2.28 ± 0.15	-0.52 ± 0.06	12.58	1.65 ± 0.06	2.75 ± 0.12
96	Gaia DR2 6719709224902437888	4873.48 ± 93.08	2.21 ± 0.17	-0.46 ± 0.07	13.01	1.60 ± 0.09	2.74 ± 0.13
97	Gaia DR2 5431861567506547072	4933.04 ± 62.21	2.56 ± 0.16	0.06 ± 0.07	11.52	1.71 ± 0.05	2.74 ± 0.12
98	Gaia DR2 5773485774490988672	4902.15 ± 70.78	2.56 ± 0.16	-0.14 ± 0.06	12.87	1.83 ± 0.06	2.73 ± 0.12
99	Gaia DR2 5373941081663359488	4638.57 ± 86.06	2.37 ± 0.18	-0.04 ± 0.07	13.28	1.55 ± 0.05	2.73 ± 0.13
100	Gaia DR2 6779777645365765504	4723.99 ± 85.78	2.50 ± 0.16	0.14 ± 0.06	12.92	1.60 ± 0.08	2.72 ± 0.12
101	Gaia DR2 5452027607189177472	4655.45 ± 72.67	2.43 ± 0.18	-0.32 ± 0.07	13.73	1.79 ± 0.08	2.71 ± 0.13
102	Gaia DR2 5675925248761091456	4851.50 ± 81.58	2.42 ± 0.18	-0.09 ± 0.07	12.76	1.62 ± 0.06	2.71 ± 0.13
103	Gaia DR2 3073566459164534016	4649.46 ± 51.93	2.44 ± 0.14	-0.01 ± 0.05	11.93	1.60 ± 0.05	2.69 ± 0.12
104	Gaia DR2 581725805395332736	4720.67 ± 81.08	2.31 ± 0.19	-0.05 ± 0.08	11.51	1.65 ± 0.04	2.68 ± 0.13
105	Gaia DR2 5391227736613349248	4779.03 ± 89.28	2.02 ± 0.18	-0.71 ± 0.07	12.43	1.87 ± 0.06	2.67 ± 0.13
106	Gaia DR2 5584495698654750080	4619.57 ± 92.18	2.17 ± 0.16	-0.44 ± 0.06	12.29	1.76 ± 0.05	2.65 ± 0.12
107	Gaia DR2 4235985476499510528	4435.76 ± 73.75	2.33 ± 0.19	-0.14 ± 0.08	13.06	1.85 ± 0.09	2.64 ± 0.13
108	Gaia DR2 5808624207616553216	4800.47 ± 83.44	2.65 ± 0.20	0.19 ± 0.08	11.00	1.63 ± 0.03	2.64 ± 0.14
109	Gaia DR2 5791204782336493184	4391.82 ± 73.05	1.94 ± 0.19	-0.10 ± 0.08	10.97	2.29 ± 0.04	2.62 ± 0.13
110	Gaia DR2 5811042927036279168	4740.72 ± 67.51	2.39 ± 0.17	-0.18 ± 0.07	12.84	1.67 ± 0.07	2.60 ± 0.12
111	Gaia DR2 6654103157075218944	4898.66 ± 76.36	2.15 ± 0.18	-0.48 ± 0.07	13.18	1.65 ± 0.07	2.59 ± 0.13
112	Gaia DR2 3466104544210064000	4838.46 ± 39.09	2.62 ± 0.12	0.04 ± 0.04	12.63	1.75 ± 0.06	2.59 ± 0.11
113	Gaia DR2 5624687732033481344	4842.71 ± 38.21	2.61 ± 0.11	0.15 ± 0.04	9.95	1.61 ± 0.02	2.59 ± 0.11
114	Gaia DR2 6779256987952631808	4827.94 ± 63.27	2.24 ± 0.16	-0.53 ± 0.06	12.61	1.78 ± 0.09	2.58 ± 0.12
115	Gaia DR2 3470350896772650880	4829.62 ± 58.23	2.32 ± 0.16	-0.05 ± 0.06	11.85	1.80 ± 0.06	2.58 ± 0.12
116	Gaia DR2 6091506902806438528	4928.63 ± 61.28	2.46 ± 0.16	-0.26 ± 0.06	11.67	1.62 ± 0.08	2.58 ± 0.12
117	Gaia DR2 5602534118921439488	5028.84 ± 88.91	2.50 ± 0.20	-0.18 ± 0.08	13.48	1.86 ± 0.07	2.57 ± 0.14
118	Gaia DR2 6036403911204069248	4748.28 ± 49.36	2.64 ± 0.14	0.14 ± 0.05	12.29	1.56 ± 0.05	2.56 ± 0.12
119	Gaia DR2 5373053294747925888	4229.96 ± 77.37	1.71 ± 0.20	-0.21 ± 0.08	13.92	2.48 ± 0.11	2.55 ± 0.13
120	Gaia DR2 2696081783518779520	4620.45 ± 95.71	2.22 ± 0.20	-0.21 ± 0.08	13.24	1.81 ± 0.12	2.55 ± 0.14

Table 3 – continued

S.No.	Object ID	Teff (K)	$\log g$ (dex)	[Fe/H] (dex)	m_v (mag)	L/L_\odot (dex)	A(Li) (dex)
121	Gaia DR2 5915006974134206080	4624.17 ± 68.64	2.20 ± 0.17	-0.14 ± 0.07	12.87	1.64 ± 0.09	2.55 ± 0.13
122	Gaia DR2 5807050222360066304	4749.61 ± 96.47	2.30 ± 0.19	0.03 ± 0.08	13.47	1.64 ± 0.04	2.54 ± 0.13
123	Gaia DR2 6139263125199366400	5166.11 ± 80.37	2.40 ± 0.19	-0.40 ± 0.08	13.32	1.55 ± 0.06	2.54 ± 0.13
124	Gaia DR2 5817665315632544384	5049.77 ± 94.53	2.57 ± 0.19	-0.33 ± 0.08	11.81	1.78 ± 0.06	2.53 ± 0.13
125	Gaia DR2 6755428784277693568	4698.75 ± 66.16	2.59 ± 0.18	0.14 ± 0.08	11.84	1.58 ± 0.05	2.53 ± 0.13
126	Gaia DR2 3011575439538999296	4857.51 ± 90.29	2.32 ± 0.17	-0.13 ± 0.07	12.86	1.35 ± 0.34	2.52 ± 0.13
127	Gaia DR2 5436690382057729408	4872.04 ± 83.56	2.42 ± 0.19	-0.01 ± 0.08	13.46	1.71 ± 0.05	2.51 ± 0.13
128	Gaia DR2 5707005521902321536	4746.37 ± 68.27	2.60 ± 0.18	0.09 ± 0.07	13.08	1.77 ± 0.09	2.51 ± 0.13
129	Gaia DR2 6708545574104290688	4941.86 ± 78.34	2.32 ± 0.18	-0.55 ± 0.07	13.55	1.71 ± 0.11	2.50 ± 0.13
130	Gaia DR2 6133545699095132032	4918.91 ± 81.14	2.54 ± 0.19	-0.10 ± 0.08	13.38	1.78 ± 0.10	2.50 ± 0.13
131	Gaia DR2 6402728307604533632	4746.04 ± 75.30	2.49 ± 0.18	0.15 ± 0.08	13.03	1.60 ± 0.07	2.50 ± 0.13
132	Gaia DR2 4377588177421757440	4710.89 ± 76.75	2.22 ± 0.18	-0.25 ± 0.08	13.49	1.40 ± 0.04	2.50 ± 0.13
133	Gaia DR2 6086711932594628352	4740.37 ± 55.21	2.78 ± 0.16	0.28 ± 0.06	12.33	1.54 ± 0.06	2.50 ± 0.12
134	Gaia DR2 4168620151412529536	4560.09 ± 69.08	2.75 ± 0.18	0.22 ± 0.07	13.01	1.35 ± 0.06	2.50 ± 0.13
135	Gaia DR2 6357806896762379904	4155.81 ± 69.59	1.49 ± 0.19	-0.55 ± 0.08	12.35	2.60 ± 0.11	2.49 ± 0.13
136	Gaia DR2 6711980899405600896	4985.90 ± 89.22	2.77 ± 0.18	-0.29 ± 0.07	11.79	1.59 ± 0.04	2.49 ± 0.13
137	Gaia DR2 5922073123050467200	4685.69 ± 54.79	2.01 ± 0.15	-0.18 ± 0.06	10.15	2.24 ± 0.04	2.49 ± 0.12
138	Gaia DR2 6650476658491541376	4721.10 ± 43.90	2.48 ± 0.13	0.10 ± 0.05	12.14	1.86 ± 0.07	2.48 ± 0.11
139	Gaia DR2 2941562426030898816	4915.92 ± 56.97	2.80 ± 0.17	0.19 ± 0.07	12.09	1.65 ± 0.05	2.48 ± 0.12
140	Gaia DR2 5791281541991683200	4727.44 ± 78.48	2.49 ± 0.20	0.15 ± 0.08	13.78	1.51 ± 0.04	2.47 ± 0.13
141	Gaia DR2 5362422391691840768	4772.38 ± 61.90	2.61 ± 0.17	-0.02 ± 0.07	13.01	1.66 ± 0.06	2.47 ± 0.13
142	Gaia DR2 5780764743325202048	4605.54 ± 62.68	2.19 ± 0.15	-0.51 ± 0.06	12.76	1.94 ± 0.06	2.46 ± 0.12
143	Gaia DR2 4620358661206107776	4725.09 ± 71.84	2.53 ± 0.19	0.25 ± 0.08	12.92	1.48 ± 0.04	2.46 ± 0.13
144	Gaia DR2 5467980455756182656	4934.78 ± 85.21	2.32 ± 0.19	-0.52 ± 0.08	13.68	1.81 ± 0.08	2.45 ± 0.13
145	Gaia DR2 5224684057518392960	4697.79 ± 56.45	2.22 ± 0.15	-0.07 ± 0.06	12.38	2.03 ± 0.05	2.45 ± 0.12
146	Gaia DR2 6141920541724000000	4827.23 ± 66.59	2.43 ± 0.17	-0.10 ± 0.07	13.03	1.63 ± 0.08	2.45 ± 0.13
147	Gaia DR2 5370859734689721600	4809.22 ± 64.08	2.55 ± 0.18	0.08 ± 0.07	12.61	1.72 ± 0.05	2.45 ± 0.13
148	Gaia DR2 2706959522635043968	4728.07 ± 58.88	2.46 ± 0.16	-0.01 ± 0.06	12.31	1.80 ± 0.11	2.45 ± 0.12
149	Gaia DR2 5436262049261115008	4249.33 ± 31.71	1.52 ± 0.10	-0.25 ± 0.03	9.75	2.60 ± 0.04	2.44 ± 0.11
150	Gaia DR2 4487925023966389376	4480.22 ± 65.82	2.48 ± 0.18	-0.08 ± 0.08	13.46	1.77 ± 0.08	2.43 ± 0.13
151	Gaia DR2 6702531009288403712	4897.72 ± 68.30	2.38 ± 0.17	-0.21 ± 0.07	11.73	1.54 ± 0.05	2.43 ± 0.13
152	Gaia DR2 5914068472234966016	4717.91 ± 86.67	2.75 ± 0.19	0.13 ± 0.08	13.71	1.59 ± 0.06	2.42 ± 0.13
153	Gaia DR2 5421023814530120704	4778.86 ± 66.32	2.67 ± 0.18	0.20 ± 0.07	12.69	1.55 ± 0.05	2.42 ± 0.13
154	Gaia DR2 6635029069878586112	4441.37 ± 49.88	1.97 ± 0.15	-0.37 ± 0.06	10.63	1.91 ± 0.04	2.42 ± 0.12
155	Gaia DR2 6157593667660508800	4743.33 ± 77.33	2.20 ± 0.19	-0.32 ± 0.08	13.80	1.65 ± 0.12	2.41 ± 0.13
156	Gaia DR2 5792476539327714816	4690.75 ± 76.60	2.22 ± 0.18	-0.35 ± 0.07	13.53	1.68 ± 0.04	2.41 ± 0.13
157	Gaia DR2 5633145995807169664	4755.24 ± 57.81	2.57 ± 0.17	0.15 ± 0.07	12.44	1.65 ± 0.05	2.41 ± 0.12
158	Gaia DR2 5376150928233716992	4625.72 ± 70.57	2.42 ± 0.18	0.03 ± 0.07	13.05	1.68 ± 0.06	2.40 ± 0.13
159	Gaia DR2 5909836829933180672	4729.30 ± 56.53	2.55 ± 0.16	0.10 ± 0.06	12.53	1.57 ± 0.05	2.40 ± 0.12
160	Gaia DR2 5297697956095835264	4769.33 ± 46.76	2.31 ± 0.14	-0.13 ± 0.05	10.57	1.98 ± 0.03	2.40 ± 0.12
161	Gaia DR2 6146039827677625856	4770.25 ± 69.99	2.42 ± 0.19	-0.01 ± 0.08	13.28	1.55 ± 0.12	2.39 ± 0.13
162	Gaia DR2 4047063815234837504	4798.05 ± 25.22	2.52 ± 0.08	0.05 ± 0.03	9.51	1.62 ± 0.02	2.38 ± 0.11
163	Gaia DR2 5493998989680647168	4905.04 ± 93.17	2.54 ± 0.19	-0.08 ± 0.08	13.77	1.74 ± 0.05	2.37 ± 0.13
164	Gaia DR2 5793721766308320128	4289.69 ± 96.75	1.37 ± 0.19	-0.70 ± 0.08	12.31	2.19 ± 0.07	2.36 ± 0.13
165	Gaia DR2 3459399967119296128	5054.88 ± 98.69	2.93 ± 0.19	-0.26 ± 0.08	13.82	1.48 ± 0.06	2.35 ± 0.13
166	Gaia DR2 5807253009230496256	4757.73 ± 70.24	2.30 ± 0.18	-0.06 ± 0.07	12.60	1.80 ± 0.05	2.35 ± 0.13
167	Gaia DR2 5721819516941191296	4778.66 ± 64.33	2.37 ± 0.16	-0.20 ± 0.07	12.85	1.67 ± 0.06	2.35 ± 0.12
168	Gaia DR2 4471569208692643200	4666.33 ± 59.43	2.93 ± 0.17	0.38 ± 0.07	12.44	1.42 ± 0.04	2.35 ± 0.13
169	Gaia DR2 6082568869702190720	4874.32 ± 54.17	2.29 ± 0.15	-0.10 ± 0.06	10.30	1.86 ± 0.04	2.35 ± 0.12
170	Gaia DR2 5791416507035670400	4881.80 ± 77.93	2.61 ± 0.16	-0.12 ± 0.06	10.44	1.59 ± 0.03	2.35 ± 0.12
171	Gaia DR2 4037523623386846336	4775.57 ± 60.72	2.78 ± 0.18	0.19 ± 0.07	11.47	1.56 ± 0.04	2.34 ± 0.13
172	Gaia DR2 6637733314425753984	4714.68 ± 54.08	2.17 ± 0.15	-0.28 ± 0.06	12.51	1.63 ± 0.06	2.33 ± 0.12
173	Gaia DR2 5374556498937060608	4978.66 ± 57.47	2.49 ± 0.16	-0.16 ± 0.06	11.53	1.72 ± 0.04	2.33 ± 0.12
174	Gaia DR2 5818798160506192000	4763.25 ± 65.20	2.52 ± 0.18	0.16 ± 0.07	11.84	1.59 ± 0.03	2.33 ± 0.13
175	Gaia DR2 5820639666385663360	4751.42 ± 69.01	2.43 ± 0.18	0.01 ± 0.07	12.79	1.53 ± 0.05	2.32 ± 0.13
176	Gaia DR2 5914162617918721280	4737.86 ± 55.13	2.56 ± 0.16	0.22 ± 0.06	12.20	1.56 ± 0.05	2.32 ± 0.12
177	Gaia DR2 6070503756813117056	4901.75 ± 56.54	2.58 ± 0.16	0.07 ± 0.06	11.12	1.75 ± 0.05	2.32 ± 0.12
178	Gaia DR2 5398253585851636992	4600.65 ± 73.73	2.37 ± 0.19	0.40 ± 0.08	13.62	1.60 ± 0.05	2.31 ± 0.13
179	Gaia DR2 5386860304630456320	5109.17 ± 71.30	2.50 ± 0.18	-0.16 ± 0.07	12.29	1.57 ± 0.04	2.31 ± 0.13
180	Gaia DR2 3253963778612870912	4758.28 ± 52.62	2.45 ± 0.15	0.07 ± 0.06	12.20	1.63 ± 0.05	2.31 ± 0.12

Table 3 – continued

S.No.	Object ID	Teff (K)	$\log g$ (dex)	[Fe/H] (dex)	m_v (mag)	L/L_\odot (dex)	A(Li) (dex)
181	Gaia DR2 5229285758501546624	4750.31 ± 56.69	2.65 ± 0.16	0.12 ± 0.06	11.59	1.54 ± 0.02	2.31 ± 0.12
182	Gaia DR2 2895200315655057920	4848.37 ± 78.74	2.32 ± 0.18	-0.25 ± 0.08	13.84	1.87 ± 0.08	2.29 ± 0.13
183	Gaia DR2 5416314370010160512	4832.31 ± 62.17	2.43 ± 0.17	0.06 ± 0.07	13.15	1.82 ± 0.09	2.29 ± 0.13
184	Gaia DR2 6078451610978783488	4886.28 ± 64.56	2.62 ± 0.18	0.19 ± 0.07	12.01	1.72 ± 0.05	2.29 ± 0.13
185	Gaia DR2 5363510495882765952	4767.83 ± 65.11	2.66 ± 0.18	0.18 ± 0.07	11.52	1.61 ± 0.04	2.29 ± 0.13
186	Gaia DR2 6715331042616800768	4773.35 ± 58.89	2.42 ± 0.16	-0.06 ± 0.07	10.89	1.60 ± 0.05	2.29 ± 0.12
187	Gaia DR2 3463132117603485440	4776.95 ± 60.66	2.65 ± 0.17	0.12 ± 0.07	12.44	1.67 ± 0.06	2.28 ± 0.13
188	Gaia DR2 6702221629897848960	4782.02 ± 64.82	2.73 ± 0.18	0.26 ± 0.07	11.69	1.58 ± 0.04	2.28 ± 0.13
189	Gaia DR2 537465112565223616	4926.98 ± 67.21	2.43 ± 0.13	-0.23 ± 0.05	9.69	1.72 ± 0.02	2.28 ± 0.11
190	Gaia DR2 5583693368703146496	4676.01 ± 82.42	2.53 ± 0.20	0.18 ± 0.09	13.62	1.61 ± 0.04	2.26 ± 0.14
191	Gaia DR2 6090505587008797440	4529.86 ± 56.53	2.40 ± 0.16	-0.16 ± 0.06	12.08	1.63 ± 0.12	2.26 ± 0.12
192	Gaia DR2 5907299672495709568	4556.19 ± 77.41	2.60 ± 0.20	0.04 ± 0.08	13.23	1.72 ± 0.08	2.25 ± 0.14
193	Gaia DR2 5797558825674487936	4752.38 ± 67.70	2.32 ± 0.15	-0.09 ± 0.06	13.29	1.63 ± 0.05	2.25 ± 0.12
194	Gaia DR2 5247038610680907904	4970.98 ± 58.13	2.53 ± 0.17	-0.07 ± 0.07	11.80	1.84 ± 0.03	2.25 ± 0.12
195	Gaia DR2 6721954290205665920	4721.79 ± 63.27	2.64 ± 0.18	0.17 ± 0.07	11.27	1.60 ± 0.03	2.24 ± 0.13
196	Gaia DR2 6703068017635031296	5057.53 ± 38.79	2.67 ± 0.12	0.14 ± 0.05	9.92	1.82 ± 0.03	2.24 ± 0.11
197	Gaia DR2 2938523856928065536	5116.55 ± 81.32	2.53 ± 0.20	-0.22 ± 0.08	13.72	1.87 ± 0.08	2.22 ± 0.14
198	Gaia DR2 6092109263376811648	4700.12 ± 69.35	2.88 ± 0.19	0.41 ± 0.08	14.00	1.43 ± 0.07	2.22 ± 0.13
199	Gaia DR2 5376045542618548736	4760.51 ± 57.42	2.47 ± 0.16	0.03 ± 0.06	12.56	1.76 ± 0.07	2.22 ± 0.12
200	Gaia DR2 54204360955050648128	4924.01 ± 59.30	2.55 ± 0.16	0.05 ± 0.06	12.21	1.69 ± 0.05	2.22 ± 0.12
201	Gaia DR2 5315969124930734464	4353.50 ± 30.73	1.69 ± 0.10	-0.03 ± 0.04	9.08	2.50 ± 0.02	2.22 ± 0.11
202	Gaia DR2 3080469021370104192	4962.88 ± 50.63	2.64 ± 0.15	0.10 ± 0.06	9.57	1.82 ± 0.02	2.21 ± 0.12
203	Gaia DR2 5415764025783016832	4782.19 ± 59.20	2.62 ± 0.17	0.21 ± 0.07	11.86	1.46 ± 0.03	2.20 ± 0.13
204	Gaia DR2 4359779314569319296	4797.57 ± 51.89	2.61 ± 0.15	0.10 ± 0.06	12.55	1.23 ± 0.05	2.20 ± 0.12
205	Gaia DR2 5793765785434358528	4805.80 ± 56.98	2.57 ± 0.17	0.22 ± 0.07	10.33	1.79 ± 0.02	2.19 ± 0.12
206	Gaia DR2 5455533812332089728	4729.53 ± 70.73	2.37 ± 0.19	0.09 ± 0.08	13.46	1.73 ± 0.05	2.18 ± 0.13
207	Gaia DR2 6735120254754428160	4830.97 ± 71.85	2.44 ± 0.19	0.12 ± 0.08	11.96	1.63 ± 0.04	2.18 ± 0.13
208	Gaia DR2 5822073571279630208	4857.42 ± 58.49	2.61 ± 0.17	0.09 ± 0.07	11.26	1.46 ± 0.03	2.17 ± 0.12
209	Gaia DR2 5678212366090166528	4863.77 ± 96.11	2.21 ± 0.20	-0.20 ± 0.08	13.47	1.96 ± 0.10	2.16 ± 0.13
210	Gaia DR2 5574618137164897536	4778.78 ± 71.35	2.26 ± 0.19	-0.19 ± 0.08	13.67	1.64 ± 0.04	2.16 ± 0.13
211	Gaia DR2 5384495873591911680	4202.23 ± 55.36	1.97 ± 0.16	-0.42 ± 0.06	12.51	2.16 ± 0.08	2.16 ± 0.12
212	Gaia DR2 6081398881948534144	4936.66 ± 49.00	2.69 ± 0.15	0.04 ± 0.06	12.36	1.67 ± 0.07	2.16 ± 0.12
213	Gaia DR2 5807170202261464704	4965.75 ± 78.40	2.26 ± 0.18	-0.28 ± 0.07	12.10	1.62 ± 0.05	2.16 ± 0.13
214	Gaia DR2 6142927861878879104	4672.71 ± 74.63	2.36 ± 0.17	-0.03 ± 0.07	11.68	1.64 ± 0.04	2.16 ± 0.12
215	Gaia DR2 5947407966903218432	4932.36 ± 84.69	2.63 ± 0.21	0.09 ± 0.09	11.17	1.72 ± 0.05	2.16 ± 0.14
216	Gaia DR2 6002549815052973568	4810.41 ± 70.69	2.41 ± 0.18	-0.05 ± 0.07	13.37	1.71 ± 0.08	2.15 ± 0.13
217	Gaia DR2 4038214773873148032	4934.93 ± 97.20	2.31 ± 0.19	-0.26 ± 0.08	13.09	1.73 ± 0.10	2.15 ± 0.13
218	Gaia DR2 3142806554658429952	4692.94 ± 85.60	2.06 ± 0.16	-0.50 ± 0.07	10.03	2.17 ± 0.04	2.15 ± 0.12
219	Gaia DR2 6703670653085991296	4619.50 ± 81.71	2.18 ± 0.19	0.14 ± 0.08	13.47	1.59 ± 0.07	2.14 ± 0.13
220	Gaia DR2 6788265634612883328	4743.15 ± 64.51	2.35 ± 0.17	-0.23 ± 0.07	13.36	1.74 ± 0.11	2.13 ± 0.13
221	Gaia DR2 6093100919786226944	4526.00 ± 89.56	2.25 ± 0.19	0.00 ± 0.08	12.82	1.63 ± 0.07	2.13 ± 0.13
222	Gaia DR2 2920138270166122496	4714.61 ± 54.33	2.67 ± 0.16	0.13 ± 0.06	11.45	1.67 ± 0.03	2.13 ± 0.12
223	Gaia DR2 5793537602412430208	4805.38 ± 75.45	2.21 ± 0.18	-0.20 ± 0.07	11.11	1.69 ± 0.02	2.13 ± 0.13
224	Gaia DR2 5918644566604591360	4920.95 ± 75.87	2.36 ± 0.17	-0.20 ± 0.07	12.88	1.86 ± 0.10	2.12 ± 0.12
225	Gaia DR2 5387273931457236096	4702.64 ± 96.11	2.46 ± 0.20	0.01 ± 0.09	13.28	1.63 ± 0.06	2.12 ± 0.14
226	Gaia DR2 5492185242170706304	4784.87 ± 68.07	2.31 ± 0.18	-0.14 ± 0.07	13.77	1.75 ± 0.05	2.11 ± 0.13
227	Gaia DR2 5806980987485756288	4985.32 ± 88.98	2.55 ± 0.19	-0.01 ± 0.08	13.98	1.54 ± 0.06	2.11 ± 0.13
228	Gaia DR2 5707045447918185728	4837.75 ± 60.39	2.30 ± 0.17	-0.13 ± 0.07	11.50	1.80 ± 0.06	2.11 ± 0.12
229	Gaia DR2 5402146368112930176	4753.24 ± 69.36	2.43 ± 0.19	0.04 ± 0.08	13.85	1.70 ± 0.09	2.09 ± 0.13
230	Gaia DR2 5463505439134617600	4621.60 ± 52.92	2.48 ± 0.16	0.05 ± 0.06	12.32	1.59 ± 0.05	2.09 ± 0.12
231	Gaia DR2 5420381669680279168	4838.36 ± 56.72	2.70 ± 0.17	0.21 ± 0.07	11.73	1.71 ± 0.04	2.09 ± 0.12
232	Gaia DR2 5947033067785490304	4555.43 ± 88.81	2.41 ± 0.19	0.11 ± 0.08	10.74	1.78 ± 0.04	2.09 ± 0.13
233	Gaia DR2 6007329426452855296	4648.61 ± 99.05	2.57 ± 0.20	0.14 ± 0.08	13.43	1.77 ± 0.11	2.08 ± 0.13
234	Gaia DR2 5913247721159217152	4897.77 ± 66.21	2.57 ± 0.18	0.07 ± 0.08	11.96	1.71 ± 0.04	2.08 ± 0.13
235	Gaia DR2 5947058837590423552	4653.73 ± 94.84	2.47 ± 0.19	-0.01 ± 0.08	11.36	1.46 ± 0.04	2.08 ± 0.13
236	Gaia DR2 5791153204062707456	4851.14 ± 68.96	2.46 ± 0.17	-0.07 ± 0.07	12.82	1.74 ± 0.05	2.07 ± 0.13
237	Gaia DR2 6041508604395805568	4676.47 ± 58.77	2.62 ± 0.17	0.17 ± 0.07	12.94	1.71 ± 0.09	2.07 ± 0.13
238	Gaia DR2 5778543321820636928	4884.46 ± 55.04	2.25 ± 0.15	-0.36 ± 0.06	12.51	1.55 ± 0.04	2.07 ± 0.12
239	Gaia DR2 6635692968739915264	4784.09 ± 89.73	2.29 ± 0.20	-0.27 ± 0.08	13.22	1.66 ± 0.12	2.06 ± 0.14
240	Gaia DR2 6458252540999316864	4781.76 ± 76.96	2.46 ± 0.18	-0.25 ± 0.07	12.99	1.84 ± 0.09	2.05 ± 0.13

Table 3 – continued

S.No.	Object ID	Teff (K)	$\log g$ (dex)	[Fe/H] (dex)	m_v (mag)	L/L_\odot (dex)	A(Li) (dex)
241	Gaia DR2 5780959051946613888	4730.17 ± 89.76	2.23 ± 0.20	-0.16 ± 0.08	12.22	2.08 ± 0.07	2.05 ± 0.13
242	Gaia DR2 6099195650177688960	4767.01 ± 78.98	2.51 ± 0.17	0.15 ± 0.07	13.32	1.64 ± 0.10	2.05 ± 0.13
243	Gaia DR2 5946690054532114688	4789.73 ± 58.84	2.89 ± 0.17	0.32 ± 0.07	13.50	1.46 ± 0.04	2.05 ± 0.13
244	Gaia DR2 1753307668590290304	4816.85 ± 43.58	2.38 ± 0.13	0.02 ± 0.05	9.99	1.77 ± 0.02	2.05 ± 0.12
245	Gaia DR2 6141356694120988416	4732.71 ± 75.38	2.59 ± 0.20	0.08 ± 0.08	12.76	1.65 ± 0.06	2.04 ± 0.13
246	Gaia DR2 5432224402043330688	4421.82 ± 57.08	2.16 ± 0.17	-0.13 ± 0.07	11.53	2.08 ± 0.05	2.04 ± 0.12
247	Gaia DR2 6635938262913646848	4752.53 ± 89.22	2.25 ± 0.20	-0.14 ± 0.09	12.42	1.52 ± 0.05	2.04 ± 0.14
248	Gaia DR2 2955975717800052352	4952.24 ± 63.53	2.28 ± 0.17	-0.47 ± 0.07	12.85	1.76 ± 0.05	2.03 ± 0.13
249	Gaia DR2 4141066630537415552	4654.90 ± 58.34	3.01 ± 0.17	0.53 ± 0.07	12.98	1.13 ± 0.04	2.03 ± 0.12
250	Gaia DR2 6092954547301602944	4709.12 ± 88.39	2.36 ± 0.20	-0.03 ± 0.08	14.04	1.70 ± 0.12	2.02 ± 0.13
251	Gaia DR2 6005001897776085248	4806.41 ± 52.60	2.52 ± 0.16	-0.04 ± 0.06	13.06	1.68 ± 0.09	2.02 ± 0.12
252	Gaia DR2 5820236081207169024	4608.44 ± 80.85	2.25 ± 0.20	-0.13 ± 0.08	11.56	1.90 ± 0.04	2.02 ± 0.13
253	Gaia DR2 5437171658912631040	4657.19 ± 65.97	2.76 ± 0.19	0.25 ± 0.08	12.48	1.54 ± 0.04	2.02 ± 0.13
254	Gaia DR2 6128997431812095360	4757.61 ± 64.48	2.59 ± 0.18	0.14 ± 0.07	13.62	1.69 ± 0.10	2.01 ± 0.13
255	Gaia DR2 5647746204556453248	4822.54 ± 70.92	2.46 ± 0.18	-0.04 ± 0.08	13.81	1.55 ± 0.07	2.01 ± 0.13
256	Gaia DR2 5455081328937070720	4679.82 ± 65.84	2.69 ± 0.18	0.17 ± 0.08	13.28	1.66 ± 0.07	2.01 ± 0.13
257	Gaia DR2 4471847934887193216	4598.36 ± 83.97	2.22 ± 0.19	0.18 ± 0.08	13.47	1.58 ± 0.06	2.01 ± 0.13
258	Gaia DR2 4139228792550926976	4620.55 ± 66.06	3.04 ± 0.19	0.56 ± 0.08	13.68	1.22 ± 0.07	2.01 ± 0.13
259	Gaia DR2 5822454964399685376	4859.07 ± 65.27	2.60 ± 0.18	0.01 ± 0.07	11.77	1.70 ± 0.04	2.01 ± 0.13
260	Gaia DR2 5703082464414878464	4701.55 ± 88.21	2.12 ± 0.19	-0.28 ± 0.08	13.47	1.84 ± 0.06	2.00 ± 0.13
261	Gaia DR2 5916687886896990592	4722.45 ± 86.31	2.59 ± 0.19	0.20 ± 0.08	13.40	1.72 ± 0.06	2.00 ± 0.13
262	Gaia DR2 6392623452147567744	4761.13 ± 38.41	2.34 ± 0.12	-0.13 ± 0.04	12.06	1.90 ± 0.04	2.00 ± 0.11
263	Gaia DR2 6009730721185313280	4081.66 ± 55.72	1.55 ± 0.16	-0.54 ± 0.06	12.51	2.42 ± 0.10	1.99 ± 0.12
264	Gaia DR2 6385288266481482880	4995.72 ± 93.12	2.33 ± 0.20	-0.48 ± 0.08	13.63	1.78 ± 0.05	1.98 ± 0.13
265	Gaia DR2 6852586167190048768	4862.05 ± 73.48	2.26 ± 0.19	-0.22 ± 0.08	12.35	1.40 ± 0.06	1.98 ± 0.13
266	Gaia DR2 6386541086965979904	4870.52 ± 58.50	2.03 ± 0.15	-0.44 ± 0.06	12.57	2.25 ± 0.08	1.96 ± 0.12
267	Gaia DR2 5561870051457417600	4761.80 ± 66.12	2.49 ± 0.18	-0.05 ± 0.07	13.60	1.60 ± 0.04	1.96 ± 0.13
268	Gaia DR2 5199361067780431616	4505.28 ± 77.93	2.48 ± 0.19	-0.04 ± 0.08	12.87	1.66 ± 0.04	1.96 ± 0.13
269	Gaia DR2 5295513776243667328	4540.07 ± 76.27	2.43 ± 0.17	0.09 ± 0.07	13.00	1.53 ± 0.03	1.96 ± 0.13
270	Gaia DR2 6037582420180899328	4803.14 ± 53.99	2.53 ± 0.16	0.00 ± 0.06	12.46	1.60 ± 0.06	1.96 ± 0.12
271	Gaia DR2 5296323669638828416	4517.15 ± 92.60	2.31 ± 0.20	-0.02 ± 0.08	13.60	1.55 ± 0.03	1.95 ± 0.13
272	Gaia DR2 6711971725355453184	4863.09 ± 47.99	2.34 ± 0.14	-0.08 ± 0.05	10.55	1.99 ± 0.04	1.95 ± 0.12
273	Gaia DR2 5296334596035138048	5170.73 ± 64.03	3.91 ± 0.19	0.34 ± 0.08	13.01	0.45 ± 0.01	1.95 ± 0.13
274	Gaia DR2 3462990284900676096	4860.85 ± 73.52	2.50 ± 0.18	0.03 ± 0.07	13.26	1.54 ± 0.08	1.94 ± 0.13
275	Gaia DR2 5915905270823073280	4783.33 ± 68.88	2.68 ± 0.18	0.08 ± 0.07	12.87	1.65 ± 0.07	1.94 ± 0.13
276	Gaia DR2 4634833353827302912	4670.48 ± 93.32	2.27 ± 0.18	-0.36 ± 0.07	12.25	1.68 ± 0.03	1.94 ± 0.13
277	Gaia DR2 6750541665543575040	5097.21 ± 63.56	3.29 ± 0.18	0.13 ± 0.07	12.36	1.06 ± 0.03	1.94 ± 0.13
278	Gaia DR2 6462052526200514048	5187.33 ± 63.99	3.75 ± 0.18	0.15 ± 0.08	13.07	0.53 ± 0.02	1.94 ± 0.13
279	Gaia DR2 6726269083069826816	4765.87 ± 58.03	2.39 ± 0.16	0.02 ± 0.06	12.50	1.67 ± 0.09	1.93 ± 0.12
280	Gaia DR2 6289585296930463744	4620.54 ± 84.76	2.17 ± 0.18	-0.35 ± 0.07	12.54	1.61 ± 0.05	1.93 ± 0.13
281	Gaia DR2 6107232942736558976	4691.86 ± 54.30	2.17 ± 0.15	-0.37 ± 0.06	12.15	1.68 ± 0.07	1.93 ± 0.12
282	Gaia DR2 6892209198998772608	4762.65 ± 65.96	2.23 ± 0.17	-0.22 ± 0.07	12.47	1.62 ± 0.07	1.92 ± 0.12
283	Gaia DR2 6086054935738957824	4698.35 ± 60.78	2.39 ± 0.17	-0.08 ± 0.07	12.37	1.65 ± 0.07	1.92 ± 0.13
284	Gaia DR2 6199127547605022080	4769.17 ± 51.71	2.73 ± 0.15	0.28 ± 0.06	12.43	1.49 ± 0.12	1.92 ± 0.12
285	Gaia DR2 5914566409254818816	4994.99 ± 42.74	2.91 ± 0.13	-0.12 ± 0.05	12.09	1.46 ± 0.04	1.92 ± 0.12
286	Gaia DR2 5228226516490660608	5003.83 ± 51.67	2.61 ± 0.16	0.03 ± 0.06	10.84	1.68 ± 0.02	1.92 ± 0.12
287	Gaia DR2 5635224523762161920	4743.68 ± 53.87	2.57 ± 0.16	0.12 ± 0.06	11.51	1.44 ± 0.03	1.92 ± 0.12
288	Gaia DR2 6791671715479344000	5004.36 ± 68.03	3.61 ± 0.19	-0.20 ± 0.08	13.34	0.52 ± 0.02	1.92 ± 0.13
289	Gaia DR2 6102457488859232768	4762.85 ± 69.87	2.43 ± 0.19	0.11 ± 0.08	12.50	1.89 ± 0.12	1.91 ± 0.13
290	Gaia DR2 6674593209090865152	4797.03 ± 68.12	2.21 ± 0.19	-0.42 ± 0.08	12.90	1.83 ± 0.12	1.90 ± 0.13
291	Gaia DR2 434538587026498816	4957.41 ± 93.14	2.40 ± 0.18	-0.27 ± 0.07	13.50	1.51 ± 0.06	1.90 ± 0.13
292	Gaia DR2 3459859459900563200	4992.39 ± 86.56	2.57 ± 0.19	-0.61 ± 0.08	14.00	1.88 ± 0.12	1.89 ± 0.13
293	Gaia DR2 5389611183939763200	4715.61 ± 55.93	2.62 ± 0.16	0.16 ± 0.06	12.76	1.58 ± 0.05	1.89 ± 0.12
294	Gaia DR2 5370788335148341504	4722.85 ± 46.58	2.15 ± 0.14	0.14 ± 0.05	10.87	1.98 ± 0.06	1.89 ± 0.12
295	Gaia DR2 3237165607464496512	4833.19 ± 69.13	2.42 ± 0.17	-0.07 ± 0.07	12.78	1.80 ± 0.08	1.88 ± 0.13
296	Gaia DR2 600898762747326360	4846.39 ± 52.15	2.47 ± 0.16	0.02 ± 0.06	12.52	1.55 ± 0.05	1.88 ± 0.12
297	Gaia DR2 6009401971515883392	4836.57 ± 63.24	2.48 ± 0.17	-0.28 ± 0.07	11.42	1.54 ± 0.06	1.88 ± 0.13
298	Gaia DR2 6112594711191576832	4810.96 ± 96.54	2.52 ± 0.20	-0.21 ± 0.08	13.25	1.75 ± 0.12	1.87 ± 0.14
299	Gaia DR2 6672740424623847936	4640.50 ± 51.23	2.05 ± 0.15	-0.52 ± 0.06	12.35	2.06 ± 0.11	1.87 ± 0.12
300	Gaia DR2 6095651580603667840	4649.68 ± 57.89	2.21 ± 0.17	-0.28 ± 0.07	11.74	2.03 ± 0.07	1.87 ± 0.12

Table 3 – *continued*

S.No.	Object ID	Teff (K)	$\log g$ (dex)	[Fe/H] (dex)	m_v (mag)	L/L_\odot (dex)	A(Li) (dex)
301	Gaia DR2 5215362333516851584	4733.07 ± 85.14	2.24 ± 0.17	-0.32 ± 0.07	12.17	1.62 ± 0.03	1.87 ± 0.13
302	Gaia DR2 5225119464122495104	4752.39 ± 55.27	2.39 ± 0.16	0.04 ± 0.06	12.58	1.47 ± 0.03	1.87 ± 0.12
303	Gaia DR2 5776561172933957888	4915.69 ± 59.25	3.14 ± 0.17	-0.04 ± 0.07	12.77	1.18 ± 0.02	1.87 ± 0.13
304	Gaia DR2 6081354901485751168	5148.79 ± 91.21	3.63 ± 0.19	0.11 ± 0.08	13.85	0.66 ± 0.03	1.87 ± 0.13
305	Gaia DR2 5369251733295804032	5196.19 ± 62.21	3.89 ± 0.18	0.24 ± 0.07	13.36	0.45 ± 0.01	1.87 ± 0.13
306	Gaia DR2 5634914908156544896	4859.02 ± 64.72	2.61 ± 0.18	0.07 ± 0.07	13.40	1.75 ± 0.05	1.86 ± 0.13
307	Gaia DR2 5370273385753624448	4684.29 ± 76.94	2.47 ± 0.20	0.07 ± 0.08	11.97	1.59 ± 0.04	1.86 ± 0.14
308	Gaia DR2 5417103819359766656	4864.13 ± 60.47	2.42 ± 0.17	-0.12 ± 0.07	11.81	1.60 ± 0.03	1.86 ± 0.13
309	Gaia DR2 578047695475401472	5198.70 ± 75.81	3.78 ± 0.20	0.37 ± 0.08	13.42	0.61 ± 0.03	1.86 ± 0.14
310	Gaia DR2 6461096844437325184	5182.80 ± 59.47	3.89 ± 0.17	0.37 ± 0.07	12.73	0.50 ± 0.02	1.86 ± 0.13
311	Gaia DR2 6735003710852578304	4930.09 ± 23.19	2.41 ± 0.08	-0.07 ± 0.03	9.26	1.91 ± 0.03	1.86 ± 0.11
312	Gaia DR2 3287566945603422848	4958.70 ± 56.60	2.28 ± 0.16	-0.57 ± 0.06	12.22	1.63 ± 0.06	1.85 ± 0.12
313	Gaia DR2 5908145815408175232	4768.10 ± 69.77	2.79 ± 0.19	0.16 ± 0.08	13.81	1.54 ± 0.06	1.84 ± 0.13
314	Gaia DR2 5243639676641783808	4986.67 ± 53.12	2.50 ± 0.16	-0.07 ± 0.06	10.85	1.76 ± 0.04	1.84 ± 0.12
315	Gaia DR2 5782285367906704512	4950.70 ± 52.05	2.61 ± 0.16	0.05 ± 0.06	10.73	1.69 ± 0.02	1.84 ± 0.12
316	Gaia DR2 6396539225371784704	5140.81 ± 57.40	3.90 ± 0.17	0.31 ± 0.07	13.06	0.40 ± 0.01	1.84 ± 0.13
317	Gaia DR2 4238064412465062912	5105.94 ± 60.57	3.57 ± 0.15	0.19 ± 0.06	10.79	0.75 ± 0.02	1.84 ± 0.12
318	Gaia DR2 5445306464409127424	4730.57 ± 53.13	2.80 ± 0.16	0.34 ± 0.06	13.18	1.52 ± 0.06	1.83 ± 0.12
319	Gaia DR2 6069512787599338112	4888.85 ± 64.78	2.37 ± 0.18	-0.08 ± 0.07	10.99	1.58 ± 0.05	1.83 ± 0.13
320	Gaia DR2 5590608811508112384	4917.13 ± 62.39	2.54 ± 0.18	-0.04 ± 0.07	12.80	1.63 ± 0.05	1.82 ± 0.13
321	Gaia DR2 6135018975959484544	4853.30 ± 58.58	2.48 ± 0.17	0.03 ± 0.07	12.67	1.52 ± 0.07	1.82 ± 0.12
322	Gaia DR2 4297442541500760320	4819.18 ± 50.32	2.55 ± 0.15	0.04 ± 0.06	11.17	1.74 ± 0.06	1.82 ± 0.12
323	Gaia DR2 6105298077149947776	5193.09 ± 68.19	3.89 ± 0.19	0.32 ± 0.08	13.91	0.47 ± 0.03	1.82 ± 0.13
324	Gaia DR2 2903941845411604224	5152.86 ± 61.57	3.91 ± 0.17	0.17 ± 0.07	13.19	0.54 ± 0.02	1.82 ± 0.13
325	Gaia DR2 5416873987069851008	4933.56 ± 62.48	3.42 ± 0.18	0.33 ± 0.07	11.55	0.88 ± 0.01	1.82 ± 0.13
326	Gaia DR2 6123223449572807424	4759.80 ± 68.24	2.50 ± 0.17	0.08 ± 0.07	13.26	1.65 ± 0.10	1.81 ± 0.12
327	Gaia DR2 3137948018934622464	4858.64 ± 65.34	2.45 ± 0.16	-0.20 ± 0.06	10.99	1.83 ± 0.05	1.81 ± 0.12
328	Gaia DR2 6082171735546777856	4830.19 ± 54.79	2.73 ± 0.16	0.18 ± 0.06	11.24	1.61 ± 0.07	1.81 ± 0.12
329	Gaia DR2 6385111412612497920	5191.38 ± 64.57	4.01 ± 0.16	0.34 ± 0.06	12.39	0.48 ± 0.01	1.81 ± 0.12
330	Gaia DR2 6688625417003949056	5196.40 ± 49.39	3.71 ± 0.15	-0.02 ± 0.06	12.09	0.51 ± 0.02	1.81 ± 0.12
331	Gaia DR2 6037492191509529600	4195.12 ± 74.10	1.95 ± 0.19	-0.24 ± 0.08	13.90	2.08 ± 0.11	1.80 ± 0.13
332	Gaia DR2 6396441643714574208	4512.14 ± 93.63	2.00 ± 0.20	-0.20 ± 0.08	12.94	2.07 ± 0.08	1.80 ± 0.14
333	Gaia DR2 4334137470757431680	4860.61 ± 81.18	2.79 ± 0.20	-0.04 ± 0.08	14.00	1.12 ± 0.34	1.80 ± 0.13
334	Gaia DR2 6852673513940765952	5022.58 ± 73.46	3.76 ± 0.20	0.02 ± 0.08	13.57	0.35 ± 0.02	1.80 ± 0.14
335	Gaia DR2 3461057652697403776	5190.11 ± 62.03	3.85 ± 0.18	0.38 ± 0.07	12.68	0.51 ± 0.04	1.80 ± 0.13